Thesis (FALL 2017)
Report on

Simulation of Atomic level Width Controlled Graphene Nanoribbon Field Effect Transistors and An Ab Initio Study of H_2O molecules Adsorption on Semiconducting GNR

Inspiring Excellence

Thesis Group Members:

Abrar Mohammad Ali	ID: 13301008
Devleena Gharami	ID: 13121121
Niger Sultana Mimi	ID: 13121132

Thesis Supervisor: **Dr. Md. Khalilur Rhaman**

Thesis Co-Supervisor: **Shifur Rahman Shakil**

DECLARATION

We hereby declare that the thesis titled "**Simulation of Atomic level Width Controlled Graphene Nanoribbon Field Effect Transistors and An Ab Initio Study of H_2O molecules Adsorption on Semiconducting GNR**" is submitted to the Department of Electrical and Electronic Engineering and Department of Computer Science and Engineering of BRAC University in partial fulfilment of the Bachelor of Science in Electrical and Electronic Engineering. This is our original work and was not submitted elsewhere for the award of any other degree or any other publication.

Date:

Dr. Md. Khalilur Rhaman
Thesis Supervisor

_ _

Shifur Rahman Shakil
Thesis Co-Supervisor

_ _

_ _ _ _ _ _ _ _ _ _ _ _ _ _ _ _ _ _

Abrar Mohammad Ali
ID:13301008

_ _ _ _ _ _ _ _ _ _ _ _ _ _ _ _ _ _

Devleena Gharami
ID: 13121121

_ _ _ _ _ _ _ _ _ _ _ _ _ _ _ _ _ _

_

Niger Sultana Mimi
ID:13121132

ACKNOWLEDGEMENTS

First of all we would like to thank The Almighty for giving us the strength and patience to complete this thesis.

We would like to thank our supervisor Dr. Md. Khalilur Rhaman who constantly encouraged us with kindness and patience and helped us to bloom whenever we faced difficulties. Special gratitude to our co-supervisor Shifur Rahman Shakil for giving us the core understanding of basics and concepts of our work. The completion of our thesis would not be possible without their constant encouragement and expert advice throughout the thesis process. We would also like express my gratitude to the other members of the thesis committee for taking the time to evaluate our work.

Last but not the least we humbly thankful to our family and friends for their support and appreciation.

To our parents….

Table of Contents

LIST OF FIGURES

LIST OF TABLES

ABBREVIATIONS

AGNR	:	Armchair Graphene Nanoribbons
DDOS	:	Device Density of States
DFT	:	Density functional theory
DNA	:	Deoxyribonucleic Acid
FET	:	Field-Effect Transistor
FCI	:	Full Configuration Interaction
GNR	:	Graphene Nanoribbon
HAGNR	:	Hydrogenated Armchair Graphene Nanoribbons
HOMO	:	Highest Occupied Molecular Orbital
HF	:	Hartree Fock
LOMO	:	Lowest Occupied Molecular Orbital
NEGF	:	Non-Equilibrium Green's Functions
NEGF	:	Nonequilibrium Green's Function
OLED	:	Organic Light Emitting Diodes
PECVD	:	Plasma Enhanced Chemical Vapor Deposition
RH	:	Relative Humidity
SCF	:	Self Consistent Field
TEM	:	Transmission Electron Microscopy

Abstract

Two Dimensional (2D) Graphene NanoRibbon (GNR) based devices have grabbed the attention of scientists associated with different fields of science and technology due to their unique structural, mechanical and electronic properties. The potential uses of those materials can be for chemical vapor sensors, photo sensors, high performance photo detectors and field effect transistor. Our research is characterized by modelling graphene devices and differing their atomic level width. Next, we observed the induced quantum transport properties and their effects in nanoscale semiconductor devices. Moreover, we analyzed the molecular adsorption process on graphene and observed the changes in sensor properties. The simulated results are then implemented in the circuit simulation to evaluated the quantum mechanical robustness of the classical functionality of digital circuits designed by the modern nanotechnology.

Introduction

According to recent research the composition of atoms and molecules in different materials as well as their dimensionalities play an important role governing their fundamental chemical and electronic properties Graphene, the 'rising star' of modern nanotechnology and materials science is one of them. For around sixty years, graphene has been used merely for analyzing properties of carbon based material theoretically as it is the basic building block of graphitic materials. Although known as a integral part of 3D bulk material, graphene was presumed not to exist, considered as a mere theoretically existed material also believed to be unstable in free state [3]. Later, it became possible to isolate single two dimensional atomic layers of atoms. Andre Geim and Konstantin Novoselov won the Nobel Prize in 2010 in Physics for this phenomenal experiments regarding the 2D graphene [3]. The covalent bond C-C is considered as the strongest bond in nature giving them remarkable mechanical strain properties. It also provides excellent electrical, magnetic, thermal, optical properties. Along with ballistic electron transport, the quantum Hall effect[16], high carrier mobility,[17] band gap tunability cause this material to be a promising candidate for diverse research based on nanoelectronic applications.

Monolayer of Carbon sheet which honeycomb lattice is tightly packed with two dimensional carbon atoms is known as Graphene.Such an atomic structure is defined by two types of bonds within the sp^2 hybridization [13]. From the four valence orbitals of the carbon atom (the 2s, $2p_x$, $2p_y$, and $2p_z$ orbitals, where $\bar{z}$ is the direction perpendicular to the sheet), the s, p_x, p_y orbitals combine to form the in-plane σ (bonding or occupied) and $\sigma*$ (antibonding or unoccupied) orbitals. Such orbitals are even with respect to the planar symmetry. The σ bonds are strongly covalent bonds determining the energetic stability and the elastic properties of graphene [19]. Moreover, electron transport in Graphene is described by a Dirac-like equation [14]. Energy dispersion relation in graphene is linear ar Dirac-points, so electrons in graphene behave as massless fermions and travel through the lattice with long mean free path, ensuring higher electron mobility [18]. Only one atom thick in dimension and with an atypical electronic

spectrum, graphene has proven to be a very fruitful table-top experiment demonstrating never before seen quantum relativistic phenomena in terms of high-energy, low-dimensional physics.

The electrical conductivity of graphene devices can be changed due to gas molecule adsorbed on surface and acting as donors and acceptors [9]. The following properties of graphene make it possible to increase the sensitivity to the final limit even with the chance of detecting individual molecules. First, graphene is a 2D material with a surface with almost no volume, which causes the maximization of the effect of surface dopants [15].It is highly conductive with low Johnson noise in the limit of no charge carriers[14]. Moreover, it has a few crystal defects, which ensures a low level of excess noise caused by thermal switching[20]. All these features take part to make a unique combination that maximizes the signal-to-noise ratio to a level sufficient for detecting changes in a local concentration by less than one electron charge at room temperature [8].

The outline of our work is as follows, initially the electronic structure of unpatterned Graphene and Graphene nanoribbon (GNR) will be discussed along with their basic properties. Previous researches based on this material and the implementations and various application in different will also be included in the chapter. Simulation procedures of calculating the quantum transport properties with detailed explanations will be provided next where Density functional theory (DFT) along with non-equilibrium Green's Functions (NEGF) formalisms are briefly outlined in order to predict the non-equilibrium quantum transport properties from atomistic approach. We have worked on four types of armchair GNR devices differing the number of carbon atoms along the width which show various properties for being used as resistance or FET along with other uses. Through some experiments it was found that, water molecule adsorbed on GNR cause defects in it that assist to create electron-tunneling of the bandgap hence widening of graphene band gap to 0.206 eV [21]. Hence, the conductivity of the suitable device can be increased by using adsorption and it can bring changes in resistivity to increase the performance. Our simulation work was focused on to analyze the electronic and transport properties of these systems such as Conductivity (G), Device Density of States (DDOS), I-V characteristics (IV). Then we used ab-initio method with self consistent calculation to analyze the adsorption of H_2O

on armchair GNR. The optimal adsorption position and orientation of the molecule on the graphene surface are determined and the adsorption energies are calculated. The highest occupied molecular orbitals and lowest unoccupied molecular orbitals (HOMO and LUMO) were introduced to analyze their charge transfer mechanism.

SIGNIFICANCE OF GRAPHENE

Basic Structure of Graphene:

In case of graphene its electronic structure rapidly evolves with the number of layers, approaching the 3D limit of graphite at 10 layers. On top of this, graphene and its bilayer, sometimes referred to as zero-overlap semimetals, are both zero-gap semiconductors with one type of electron and one type of hole. In case of three or more layers(single-, double- and few-layer graphene), several charge carriers appear and the conduction and valence bands start notably overlapping which let them be perceived as three different types of 2D crystals. Buckyballs show 0D features, rolled tube shows the 1D features or 3D by sacking into graphite.

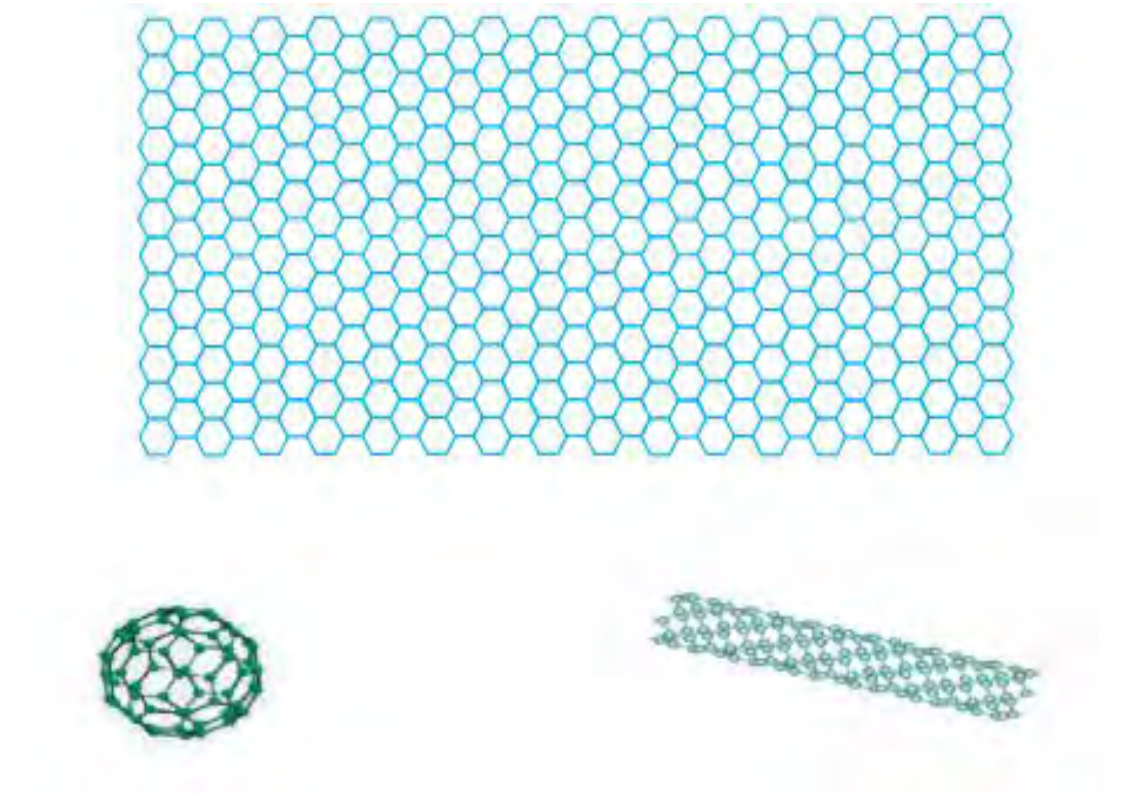

Fig. 1: Graphene 0D, 2D and 3D structure[13]

At 2004 , graphene was first being isolated as a result its theoretical revolution makes more sense to have high functioning graphene devices at this stage of nanoscale device.

Graphene Nanoribbon (GNR)

Multiple types of Graphene nanoribbons exist classified by the shape of their edges i.e. armchair and zigzag nanoribbons which depends on the chirality. The conductivity of these GNRs is highly dependent on their width and edge types. Tight-binding calculations show that armchair GNRs will be metallic when n=(3*m-1) where m is an integer or otherwise semiconducting. Moreover, the energy band gap decreases as n increases. On the other hand zigzag GNRs are all metallic primarily because of the additional energy states appearing on their edges.

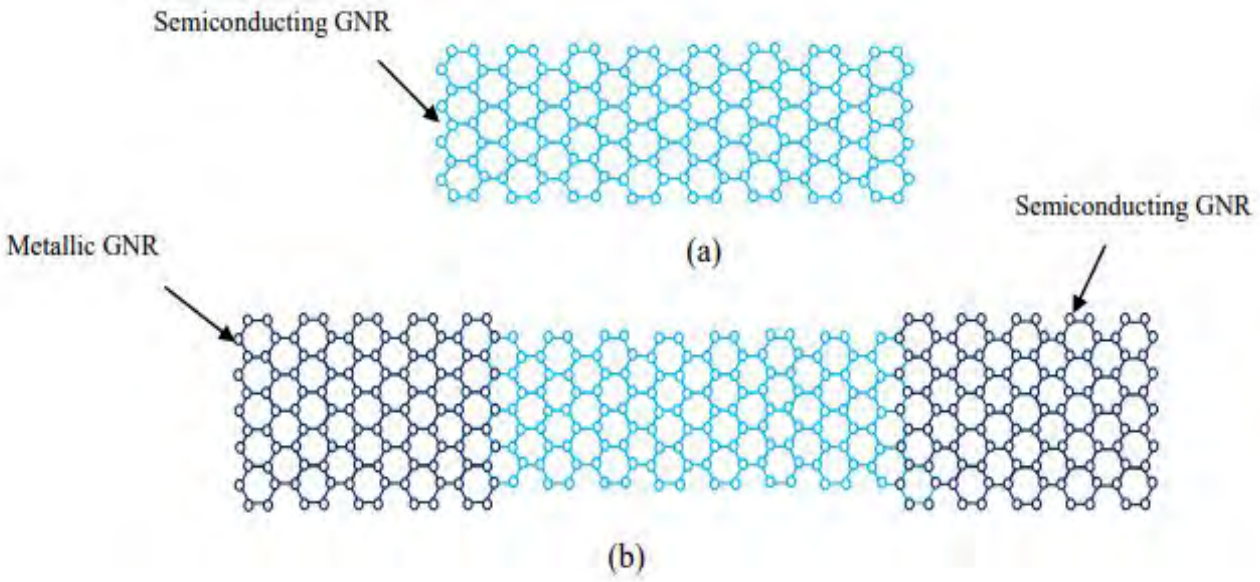

Fig.2: (a) Armchair GNR, (b) metallic and semiconducting armchair cascaded GNR[13]

PROPERTIES OF GRAPHENE

Structural Properties:

Sp2 hybridization and tightly packed carbon atom's show the stability characteristic for graphene where Px and Py makes the sigma bond to create Sp2 hybridization and the rest Pz creates pi bond which is the key of allowing free electron to show further important activities for graphene. Diffraction characteristic can be seen at graphene sheets for layered graphite in solid. TEM studies show the crystallization 2D model in this perspective . It can repair holes when it exposed to molecules containing hydrocarbons. Atoms are also perfectly aligned as hexagons.

Band Structure:

Graphene- a honeycomb lattice created by a monolayer of carbon atoms is creating a great matter of interest in the field of Solid State Physics in recent days. Each carbon atom is connected to three other carbon atoms by which they share electrons among them. Comparatively, a low lying band gets formed by the three valence electrons out of all four valence electrons. The left one electron that contains the the "P_2-orbital" character, stays perpendicular to the graphene place.

The graphene band structure can be described as the tight binding one which was introduced by Wallace. The very unprecedented features shown by this band structure: The valence bands and the conduction bands do not overlap each-other and are certainly not even separated by a band gap. Because of the bent of the energy bands, energy masses get created which coincides to zero effective mass. In the first Brillouin zone, the connection points of the cones are known as Dirac points. In the vicinity of the Dirac Points in most semiconductors, the electron dispersion is conical asn not parabolic. However, the group velocity V_g= E(k) does not depend on the energy.

Graphene does not contain any gaps and the Fermi level for undoped graphene lies specifically at the intersection points. So a relativistic dynamic equation can be written for the excitation since the dispersion curve has in common with ultra-relativistic particles. From the tight binding model this equation can be derived and the resulting equation is apparently the Dirac equation for mass less particles.

Electronic:

Graphene has an unique property of zero band gap including both holes and electrons as charge carriers with a large amount of electrical conductivity. The electron distribution of Carbon atom (C_6=$1s^2 2s^2 2p^2$) describes that there are four outer shell electrons available for chemical bonding. But unlike Carbon, in graphene each individual atom is straightly connected to three other Carbon atom from the surroundings in the 2D plane where one electron remains free in the 3D for electronic conduction. These highly mobile electrons (known as π electrons) staying at the top and bottom of the graphene sheet, help to enhance the carbon to bonds in graphene.

In Graphene, at Direc points holes (known as Dirac fermions or Graphinos) and electrons have zero effective mass because of the linear energy movement relation for low energies near each of the six corners (known as Dirac Points) of the Brillouin zone. Hense, doping can change Fermi level to develop a material that provides a better conducting electricity than copper at room temperature.

According to the tests, Graphene is characterized by a high amount of electronic mobility (more than 15,000 cm2·V−1·s−1 and theoretically, potential limits of 200,000 cm2·V−1·s−1; limited by the scattering of graphene's acoustic photons). It describes that due to having a lack of mass, the charge carriers of Graphene can travel sub-micrometer distances without scattering (which is known as ballistic transport) and can really act very much like photons in their mobility.

Mechanical strength:

Graphene has been predicted to have an innate tensile strength that is so higher than any other materials similar to materials like graphite. It is considered as the the strongest of earth with having the strength of its 0.142 Nm-long Carbon bonds. Its tensile strength is 130 GPa which is a lot stronger than steel (0.4 GPa). Moreover, Graphene is very light as well having a weight of 0.77 milligrams per square meter. Its elastic properties helps it to retain its initial shape after having any strains. So we can really make semiconductors highly flexible and nearly unbreakable by creating holes in a Graphene sheet and dope those with desired impurities.

Optical:

Due to having its aforesaid electronic properties, being only 1 atom thick Graphene has an unique ability to absorb 2.3% as the electrons act almost like messless charge carriers along with a very high mobility. Graphene has an opacity of $\pi\alpha \approx 2.3\%$ which is equal to a universal dynamic conductivity value of $G=e2/4\hbar$ (±3%) over the visible frequency range. When the nonlinear input optical intensity (known as saturable absorption) of Graphene is above the threshold value (known as saturation fluence), beauce of these unique characteristics it shows a remarkable absorption capability. Due to having this optical absorption capability and zero band gap, graphene can readily be saturated under strong excitation above the infrared region; which makes Graphene widely applicable in ultrafast photonics. The microwave saturable absorption in graphene describes the possibility of having terahertz photonics devices and graphene microwave such as modulator, microwave signal processing, broadband wireless access networks, polarizer and microwave saturable absorber.

Thermal:

The thermal conductivity of Graphene is much higher than any other carbon structures like Carbon Nanotubes, graphite and diamond. So it is considered to be the perfect thermal conductor of all having an isotopic ballistic thermal conductance. Again, the 3D version of graphene shows 5 times smaller thermal conductivity. This occurrence is subordinated by the existence of elastic waves propagating in the graphene lattice which is known as phonons. This thermal conductivity in graphene is very much important in devices based on graphene. The thermal conductivity at near-room temperature of graphene was found between (4.84±0.44) × 103 to (5.30±0.48) × 103 W·m−1·K−1. These measurement found by a non-contact technique are in excess of the measured for diamonds or carbon nanotubes. Moreover, the ^{12}C graphene contains higher conductivity than either a 50:50 isotope or 99:1 ration, which means ^{12}C and ^{13}C has a remarkable impact on thermal conductivity, which can be shown according to the Wiedemann-Franz law that the conduction is dominated by phonon. However, for a gated graphene strip, the Fermi level can be shifted much higher than k_BT caused by the applied gate bias to increase and dominate over the phonon contribution at low temperature. Graphene has an isotopic ballistic thermal conductance.

The 3D version of Graphene that has a thermal conductivity of more than 1000 W·m−1·K−1 while Graphite has a smaller conductivity due to having the weak binding between the basal place in the c-axis along with the larger lattice spacing.

SOME PREVIOUS WORKS BASED ON GRAPHENE

In these recent years in industrial, agricultural and human activities, measurement and control of environmental humidity has grabbed the attention of modern science and technology. From the recent past till date various types of humidity sensors have been developed over various courses. To meet the required needs of this massive population humidity sensors having higher sensitivity, wider detection range as well as quicker response and shorter recovery times are being manufactured each passing moment. To turn these goal into reality, considerable attentions has been rendered towards the development of humidity sensitive materials or elements, especially nanomaterials due to their high surface to volume ratio. Materials like silicon, 1D carbon, ceramic nanomaterials, semiconductor nanoparticles and metal oxide nanowires and nanofilms are getting investigated. Using these materials the progress remains limited to the day.

However graphene is a novel humidity sensing material that possesses high and even sensitivity for the full range of humidity. Graphene is consisted of 2D monolayer of sp2-bonded carbon atoms that shows an incredible characteristics in thermal, mechanical and electrical properties. It represents a remarkable potential for ultrasensitive detection and sensors that are based on graphene which have raised significant interest among the modern science arena. These sensors show very high and effective sensitivity to gases including NO2, NH3 and many more.

In these recent years many researches have been done on the applicability of graphene in terms of being used as gas sensors with a property based on the sensitivity, selectivity and stability of graphene sensors in artificial conditions. In one insightful work Electrical Conductivity of Hydrogenated Armchair Nanoribbon as a Gas Sensor Using Non-Equilibrium Green's Function Method was done with very promising results. The armchair graphene nanoribbons (AGNR) are focused on in this work which is hydrogenated from their edges which are then called hydrogenated AGNR (HAGNR). Here a HAGNR has been considered where hydrogen or oxygen molecules were absorbed on its surface. The results show that at low adsorption

concentrations, more adsorption of hydrogen or oxygen molecules leads to the increase of conductivity of the system, while at high adsorption concentrations, more adsorption leads to the reduction of conductivity. Therefore, conductivity could identify the percentage of adsorbed gas molecules. In the clean HAGNR the upper (lower) edge sites construct metallic regions separated by semiconducting regions. Adsorption of hydrogen/oxygen molecule by metallic sites leads to a reduction of current, while those by semiconducting sites lead to an increase in current. The adsorption of hydrogen/oxygen by semiconducting sites converts these sites to metallic sites. Hence these adsorption increases current while the adsorption of hydrogen/oxygen by metallic sites reduces the current.

Researchers have also discovered that at high adsorption concentration, adsorption by semiconducting sites including increased energy gap increases current more than smaller energy gap semiconductor sites, and adsorption by more metallic sites decreases current with respect to those sites with low metallic characteristics.

Here in this study various interesting facts about graphene came up which highly encourages it to be used as a gas sensor with a lot of precision. Using the NEGF method effects of gas adsorption on the electronic properties of HAGNR was investigated in this paper. It was found that at low adsorption concentration, adsorption by metallic HAGNR sites decreases current, while adsorption by semiconducting HAGNR sites increases current. However, at high adsorption concentration, the whole system becomes metallic, so by increasing adsorption concentration, current always decreases. Also at low adsorption the conductivity of the system increases by increasing adsorption, while at high adsorptions, the conductivity decreases by increasing adsorption.

Graphene is getting used widely as a sensor in Civil Engineering as well, used as a Graphene Based Resistive Humidity sensor for In-Situ Monitoring of Drying Shrinkage and Intrinsic Permeability in Concrete has been suggested. In this work the researchers have discussed about the relevance and feasibility of embedding relative humidity nanosensors within concrete where

the continuous and localized knowledge of relative humidity within a concrete structure could provide some in depth information about drying shrinkage. It could also enhance the actual measurement of the inherent permeability leading to the correct assessment of structural durability. Here a low-cost down scalable resistive device made of a 10 nm graphene sheet grown directly on glass has been proposed atop which are ink-jet printed silver electrodes. The device resistance increase efficiently with relative humidity (RH) especially above 40% RH.

Drying shrinkage is present here for significant degradation of concrete material and it depends strongly on both capillary pressure and liquid water saturation. Denoting $\mathcal{E}$ as the drying shrinkage the relationship is given below:

$$d\mathcal{E} = \frac{bS}{K} dp = - \frac{bpRT}{KM} S \frac{dh}{h} \quad (1)$$

Where b is the Biot's Co-efficient and K is the Bulk Modules of the drained material. If the relative humidity repartition h(x,t) from the embedded sensors are known then using the above equation and an integration step can be used to yield the total shrinkage. Previously the external relative humidity was used to determine the drying shrinkage but with the help of this device a more specific measure is possible of the relative humidity inside of the concrete which allows a more specific measure of the durability of the concrete. Also with this device a continuous measurement of shrinkage is achieved and consequently an improved prediction of shrinkage related cracking is attainable.

Another work on graphene has analyzed the Influence of Humidity on the Resistance Structure with graphene Sensor layers. In the atmosphere, the fluctuation of the steam content in air and the unknown ability of sensors layers to absorb it are the most intervening factor in the actual operation of devices due to the detection of gases. According to this work, the DFT (Density Functional Theory) analysis has been taken place to describe that the absorbed water molecules on graphene causes defect in it that simplifies the electron tunneling of the band gap and cause widening of band gap in graphene.

As graphene is a hydrophilic material so when water is absorbed on its surface, the structure acts like a semiconductor along with an increased band gap in the width. So, graphene swells and shrinks in relation to the relative humidity level. The researchers believe that the resistances changing that have been observed at various humidity levels are done because of this swelling and shrinking.

To observe the sensitivity of graphene affected by NO_2 (Nitrogen Dioxide) Experiments were enacted thoroughly. At first, the sensor structure reaction with graphene on the action of moist air (5.7% humidity at 50^oC temperature) is performed and then NO_2 gas was introduced at intervals. It was observed that when only air flows through the channel and decreases when NO_2 passes through it, the resistance remained as a constant (about 11.5Ω). After the first reaction with NO_2 the structure does not regain its previous resistance. This is because when molecules of NO_2 gases are absorbed onto graphene, as bringing electrons from graphene holes are created which decreases resistance. The decreased resistance is constant and does not fade entirely after gas exchange because adsorption of NO_2 into graphene structure is constant. Part of NO_2 reacts with the absorbed water forming nitric acid which generates stable defects in graphene structure.

The same experiment was performed but with a decreased amount of humidity (4.78%) in air. The result of the sensing structure is quite faster than the previous experiment and showed a clear decrease in resistance. When temperature was increased to 120^oC and other factors remaining the same, it showed a slide increase in resistance. This increase is greater when percentage of humidity is increased in air.

VARIOUS APPLICATION OF GRAPHENE

Better Lithium-Ion Batteries: In these batteries, graphene is used as an anode. Defects in the graphene sheet provide pathways for the lithium ions to attach to the anode substrate. Both theoretically and practically it is shown that a battery using graphene on the surface of the anode takes much shorter amount of time to recharge than the conventional lithium-ion batteries.

Better Mobile Device Display Screens at a lower cost: It is proved that in OLED (Organic Light Emitting Diodes) graphene can replace indium based electrodes which is widely used in the display screen of electronic devices that requires low power consumption. So in the OLED, the usage of graphene instead of indium reduces the cost as well as eliminates the use of metals that makes a device easier to get recycled.

Using Graphene for Hydrogen Fueled Cars: Researchers have prepared graphene layers to be used in a fuel tank to increase the binding energy of Hydrogen that will provide a large amount of storage of Hydrogen resulting a lighter weight fuel tank. Which means, graphene layers can be used to develop Hydrogen fueled cars.

Ultra-Capacitors: Ultra capacitors are capacitors that store the electrical power in the capacitor by storing electrons on the graphene sheets. As graphene has a large surface, it helps to increase that electrical power a lot more and can be stored in the capacitor. Researching are predicting that these capacitors will have much more electrical storage capacity than lithium ion batteries that will take minutes than an hour to be recharged.

Lightweight Natural Gas Tanks: Researchers have developed a different observation using graphene nanoribbons and plastic as a composite material that will block the passage of gas molecules. This material shall be used in making lightweight natural gas tanks.

Low Cost Water Desalination: It is technically proven that a graphene sheet with holes can easily be used to remove ions from water. So it means that it can be used to desalinate the sea water at a lower cost, resulting more efficient and perfect desalination than the currently used reverse osmosis technique.

Lower Cost Fuel Cells: Researchers have elucidated that graphene nanoplatelets that are edge halogenated have better catalytic properties. By using Ball-milling graphene flakes, they designed the nanoplatelets in the presence of chlorine, bromine or iodine. According to their research, these halogenated nanoplatelets could replace the expensive platinum catalytic material that are getting used in fuel cells.

Efficient Dye Sensitized Solar Cells: It has been tested that using a 3D graphene instead of platinum in a dye sensitized solar cells can achieve 7.8 percent conversion of sunlight to electricity. This 3D graphene is shaped like honeycomb structure along with the sheets are held apart by lithium carbonate. It is more efficient and less time consuming.

Lower Cost Solar Cells: Researchers have designed a solar cell made of graphene as an electrode while using buckyballs and carbon nanotubes to absorb light and generate electrons. It reduces the high amount of cost for the material purpose and manufacturing processes for the general solar panels.

Chemical Sensors Effective at detecting explosives: This type of sensors have graphene sheets in the form of foam that if needed it changes resistance when low levels of vapors from chemical, like Ammonia is present.

High Frequency Transistors: Using graphene it is possible to build a very high frequency transistor at which electrons in graphene move compared to electrons in silicon. Another technique called lithography technique is getting developed based on graphene by the researchers that can be used to fabricate integrated circuits.

Sensors to Diagnose Diseases: these sensors are based on the molecules that are sensitive to a particular disease can attach to the carbon atoms in graphene. For example, researchers have discovered that graphene, strands of DNA and fluorescent molecules can be well amalgamated to diagnose diseases. A sensors is formed by attaching fluorescent molecules to single strand DNA and then attaching the DNA to graphene. When an identical single strand DNA combines with the strand on the graphene, a double strand DNA formed floats off from the graphene that increases the fluorescent level, resulting an effective sensor that can detect the same DNA for a particular disease in a sample.

Simulation

Schrodinger Equation:

The Schrodinger equation is the fundamental equation of physics for describing quantum mechanical behaviour often called as the Schrodinger Wave equation and is a partial differential equation that describes how the wave function of a physical system evolves over time. The gerenal form of Schrodinger equation is as follow:

$$E\Psi = H\Psi \tag{2.1}$$

Where H = Hamiltonian operator

Ψ = electron probability density

E = total energy

To apply the Schrodinger equation, the Hamiltonian operator for the system, accounting for the kinetic and potential energy of the particles constituting the system, then inserted into the Schrodinger equation. The resulting partial differential equation is solved for the wave function, which contains information about the system. The effective mass Hamiltonian simple relation is

$$H(k) = E_c + \frac{\hbar^2 k^2}{2mc} \tag{2.2}$$

Where E_c = Potential Energy

K = Wave number

$\hbar$ = Planck's constant/2π

Hence putting the value of Hamiltonian operator in general Schrodinger equation we get the Schrodinger equation for a single non-relativistic particle:

$$E\psi(s) = -\frac{\hbar^2}{2m}\nabla^2\psi(s) + V(s)\psi(s) \quad (2.3)$$

Here, m = Effective mass of an electron

∇^2 = Laplacian operator

$V(s)$ = Potential energy

Schrodinger wave equation is mainly used to determine the probability density function for a nanoscale device. In a bulk material where the number of atoms is in huge quantities. More atoms means more number of electrons which leads to more number of overlapping of electron orbitals among themselves when the electrons come close to each other overcoming coulomb's electrostatic force of repulsion. As a result there will be more band splitting of electron orbitals and hence the energy profile tends to become continuous. This procedure can be explained using classical mechanics. But in case when the materials tends to be in the nanometer range as for example in quantum well, there exists discrete energy levels. So this scenario cannot predict accurately to find the electron probability density function. In this case we use the Schrodinger wave equation to predict the electron density probability functions at different energy levels at different points. Then integrating the total surface over different energy states, we get the total electron probability density function.

The Density Functional Theory (DFT):

The density functional theory (DFT) is currently the most successful approach to calculate the electronic structure of matter. Its capability ranges from atoms, molecules and solids to nuclei and quantum and classical fluids. In its original formulation, DFT provides the ground state properties of a system and the electron density plays a key role. For example DFT predicts a great variety of molecular properties: molecular structures, vibrational frequencies, atomization energies, ionization energies, electric and magnetic properties, reaction paths, etc. The original

density functional theory has been generalized to deal with many different situations: spin polarized systems, multicomponent systems such as nuclei and electron hole droplets, free energy at finite temperatures, superconductors with electronic pairing mechanisms, relativistic electrons, time-dependent phenomena and excited states, bosons, molecular dynamics, etc.

The goal of almost all approaches in solid state physics is the solution of the time-independent, non-relativistic Schrodinger equation:

$$H\psi_i(x_1 x_2 ... x_N R_1 R_2 ... R_M) = E_i \psi_i(x_1 x_2 ... x_N R_1 R_2 ... R_M) \tag{3.1}$$

Here H is the Hamiltonian for a system consisting of M nuclei and N electrons.

$$H = -\frac{1}{2}\sum_{i=1}^{N}\nabla_i^2 - \frac{1}{2}\sum_{A=1}^{M}\frac{1}{M_A}\nabla_A^2 - \sum_{i=1}^{N}\sum_{A=1}^{M}\frac{Z_A}{r_{iA}} + \sum_{i=1}^{N}\sum_{j>i}^{N}\frac{1}{r_{ij}} + \sum_{A=1}^{M}\sum_{B>A}^{M}\frac{Z_A Z_B}{R_{AB}} \tag{3.2}$$

The Born-Oppenheimer Approximation:

Due to their masses the electrons move much faster than the nuclei so we can consider the electrons as moving field of the nuclei in a stationary state. Thus the nuclear kinetic energy is zero and their potential energy is merely a constant. The electronic Hamiltonian reduces to:

$$H_{elec} = -\tfrac{1}{2}\sum_{i=1}\nabla_i^2 - \sum_{i=1}^{N}\sum_{A=1}^{M}\frac{Z_A}{r_{iA}} + \sum_{i=1}^{N}\sum_{j>i}^{N}\frac{1}{r_{ij}} = T + V_{Ne} + V_{ee} \qquad (4.1)$$

The solution of the Schrodinger equation with H_{elec} is the electronic wave function elec and the electronic energy E_{elec} . The total energy E_{tot} is the sum of E_{elec} and the constant nuclear repulsion term E_{nuc}.

$$H_{elec}\Psi_{elec} = E_{elec}\Psi_{elec} \qquad (4.2)$$

$$E_{tot} = E_{elec} + E_{nuc} \qquad (4.3)$$

where $$E_{nuc} = \sum_{A=1}^{M}\sum_{B>A}^{M}\frac{Z_A Z_B}{R_{AB}} \qquad (4.4)$$

The Electron Density:

The electron density is the central quantity in DFT. It is defined as the integral over the spin coordinates of all electrons and over all but one of the spatial variables:

$$\rho(\bar{r}) = N\int ...\int \psi(x_1, x_2, ..., x_N)^2 dx_1 dx_2, ..., dx_N ..... \qquad (5)$$

The First Hohenberg-Kohn Theorem:

The first Hohenberg-Kohn theorem demonstrates that the electron density uniquely determines the Hamiltonian operator and thus all the properties of the system. This first theorem states that the external potential (r) is (to within a constant) a unique functional of (r); since, in turn $Vext(r)$ fixes H we see that the full many particle ground state is a unique functional of $\varrho(r)$.

$\varrho(r)$ determines N and $Vext(r)$ and hence all the properties of the ground state, for example the kinetic energy T[ϱ], the potential energy V [ϱ], and the total energy E[ϱ]. Now, we can write the total energy as:

$$E[\rho] = E_{Ne}[\rho] + T[\rho] = E_{ee}[\rho] = \int \rho(r) V_{Ne}(r) dr + F_{HK}[\rho] \tag{6.1}$$

$$F_{HK}[\rho] = T[\rho] + E_{ee} \tag{6.2}$$

This functional F_{HK} [ϱ] is the basis of density functional theory. If it were known we would have solved the Schrodinger equation exactly! And, since it is a universal functional completely independent of the system at hand, it applies equally well to the hydrogen atom as to gigantic molecules such as, say, DNA! F_{HK} [ϱ] contains the functional for the kinetic energy T[ϱ] and that for the electron-electron interaction,E_{ee}[ϱ].

Calculation of Different Parameters:

The Electrical Current:

$$I = \frac{2e}{h}\int_{-\infty}^{\infty} d\varepsilon Tr\{tt^{+}\}[f(\varepsilon - \frac{eV}{2}) - f(\varepsilon + \frac{eV}{2})] \quad (7.1)$$

The Device Density of States (DDOS):

$$DDOS(E) = \frac{1}{2\pi} Tr[G^{R}(\Gamma^{L} + \Gamma^{G})G^{A}] \quad (7.2)$$

Conductance(G):

$$G(E) = \frac{2q^{2}}{h} Tr[\Gamma^{L} G^{R} \Gamma^{R} G^{A}] \quad (7.3)$$

The Nonequilibrium Green's Function (NEGF) Method:

Here Graphene nanoribbon is treated as a quasi-1D conductor. For such a nanoscale system, Landauer Formula is generally used to calculate the current:

$$I = \frac{2q}{h} \int_{-\infty}^{\infty} T(E)[f(E-\mu_1) - f(E-\mu_2)]dE \tag{8.1}$$

Here *T(E)* refers to the Transmission Coefficient, *f(E)* is the Fermi-Dirac Distribution function, and $_1$ and $_2$ are used to explain the Fermi energies of the left and right contact of the conductor. The coefficient 2 is taken to consider the electron spin.

If we consider the simplest case of the thermal broadening function where temperature is 0K, the thermal broadening function becomes Dirac delta function with area equals to one. This form of Landauer formula is used to calculate the conductance of graphene nanoribbon:

$$G(E) = \frac{2q^2}{h} T(E) \tag{8.2}$$

In the Landauer formalism, the nanoscale conductor is assumed to be connected to the contacts by two uniform leads that can be viewed as quantum wires with multiple subbands. If the energy-dispersion (E-k) relation is known, a t-matrix similar to a microwave waveguide can be formulated using the scattering matrix method. The method of calculating transmission is given by,

$$T(E) = \sum_M \sum_N |t_{mn}|^2 = Tr[tt^T] \tag{8.3}$$

Here, t is the t-matrix whose element t_{nm} is the amplitude for an electron incident in mode m in lead 1 transmitting to a mode n in lead 2.

The Nonequilibrium Green's Function (NEGF) is a convenient method for calculating the transmission coefficient. The electron density was given by the electron density matrix. The density matrix is divided into left and right contributions:

$$D = D^L + D^g \tag{8.4}$$

The left density matrix contribution can be given from NEGF theory as follows:

$$D^L = \int \rho^L(\varepsilon) f\left(\frac{\varepsilon - \mu_L}{k_B T_L}\right) d\varepsilon \tag{8.5}$$

$$\rho^L(\varepsilon) = \frac{1}{2\pi} G(\varepsilon) \Gamma^L \; G^\dagger \tag{8.6}$$

Where ϱ^L in the above equation is the spectral density matrix. While there is a Nonequilibrium electron distribution in the central region, the electron distribution in the electrode is described by a Fermi function f with an electron temperature T_L.

The $G(\varepsilon)$ is the retarded Green's function and Γ^L is the broadening function of the left electrode, given in terms of the left electrode self-energy as shown below:

$$\Gamma^L = \frac{1}{i}(\Sigma^L - (\Sigma^L)^+) \tag{8.7}$$

A similar equation exists for the right density matrix contribution.

The Retarded Green's Function:

The retarded Green's function matrix is a key quantity to measure:

$$G(\varepsilon) = \frac{1}{(\varepsilon + i\delta_+)S - H} \tag{8.8}$$

Where $\delta+$ are an infinitesimal positive number and S, H the overlap and Hamiltonian matrices, respectively, of the entire system. The Green's function is only required for the central region and can be calculated from the Hamiltonian of the central region by adding the electrode self-energies:

$$G(\varepsilon) = [(\varepsilon + i\delta_+)S - H - \Sigma^L(\varepsilon) - \Sigma^R(\varepsilon)]^{-1} \tag{8.9}$$

The calculation of the Green's function of the central region at a specific energy, therefore basically requires the inversion of the Hamiltonian matrix of the central region.

The Self-Energy:

The self-energies describe the effect of the electrode states on the electronic structure of the central region. The self-energy can be calculated from the electrode Hamiltonian H. Three different methods for calculating the self-energy are provided:

Recursion Self Energy:

A semi-infinite matrix A_{LL} can be divided into

$$A_{LL} = \begin{bmatrix} A_{L'L'} & A_{L'0} \\ A_{0L'} & A_{00} \end{bmatrix} \tag{9.1}$$

$$g^{L}_{0,0} = [A_{0,0} - A_{0L`}A_{L`L`}A_{L`0}] = [A_{0,0} - A_{0,-1}g^{L`}_{-1,-1}A_{-1,0}] \tag{9.2}$$

Thus we obtain the matrix quadratic equation for $g^{L}_{0,0}$

$$g^{L}_{0,0} = [A_{0,0} - A_{0,-1}g^{L`}_{-1,-1}A_{-1,0}] \tag{9.3}$$

In the same way, the quadratic equation for $g^{R}_{M+1,M+1}$ can be obtained:

$$g^{R}_{M+1,M+1} = [A_{0,0} - A_{-1,0}g^{R}_{M+1,M+1}A_{0,-1}] \tag{9.4}$$

The matrix quadratic equation gives a simple iterative method for calculating surface green's functions. They must be calculated until self-consistency is achieved. This usually involves more than 50 iterations. Especially, when $g^{L}_{0,0}$ or $g^{R}_{M+1,M+1}$ is in the neighbourhood of singularities when several hundred iterations may be needed to get an accurate result.

An iterative scheme is developed which converges much faster. After n iterations 2*n* unit cells instead of n unit cells are taken into account. The following series of matrix equations are obtained:

$$A_{0,0}g^L_{0,0} = I - A_{0,-1}g^L_{-1,0} \tag{9.5}$$

$$A_{-1,-1}g^L_{-1,0} = \; -A_{-1,0}g^L_{0,0} - A_{-1,-2}g^L_{-2,0} \tag{9.6}$$

$$A_{-2,-2}g^L_{-1,0} = \; -A_{-2,-1}g^L_{-1,0} - A_{-2,-1}g^L_{-1,0} - A_{-2,-3}g^L_{-3,0} \tag{9.7}$$

The general term can be written as:

$$g^L_{-n,0} = A^{-1}_{0,0}(-A_{0,-1}g^L_{-n+1,0} - A_{0,-1}g^L_{-n-n,0}) = t_0 g^L_{-n+1,0} + \tilde{t_0} g^L_{-n-1,0} \tag{9.8}$$

where, $t_0 = A^{-1}_{0,0}A_{0,-1}$ and $\tilde{t_0} = \; -A^{-1}_{0,0}A_{0,-1}$

$$g_{-n,0} = t_0(t_0 g^L_{-n+2,0} + \tilde{t_0} g^L_{-n,0}) + \tilde{t_0}(t_0 g^L_{-n,0} + \tilde{t_0} g^L_{-n-2,0}) \tag{9.9}$$

$$g^L_{-n,0} = t_1 g^L_{-n+2,0} + \tilde{t_1} g^L_{-n-2,0} \tag{9.10}$$

with $t_1 = (I - t_0\tilde{t_0} - \tilde{t_0}t_0)^{-1}t_0^2$ and $\tilde{t_1} = (I - t_0\tilde{t_0} - \tilde{t_0}t_0)^{-1}\tilde{t_0}^2$

The process can be repeated iteratively to obtain:

$$g^L_{-n,0} = t_i g^L_{-n+2^i,0} + \tilde{t_i} g^L_{-n-2^i,0} \tag{9.11}$$

The following chain of equations are obtained:

$$g^L_{-1,0} = t_0 g^L_{0,0} + \tilde{t_0} g^L_{-2,0} \tag{9.12}$$

$$g^L_{-2,0} = t_1 g^L_{0,0} + \tilde{t_0} g^L_{-4,0} . \quad (9.13)$$

$$g^L_{-2^n,0} = t_n g^L_{0,0} + \tilde{t_n} g^L_{-2^{n+1},0} \quad (9.14)$$

The Poisson's Equation:

Once the non-equilibrium density is obtained the next step in the self-consistent calculation is calculating the effective potential. The calculation of the exchange-correlation potential is straightforward since it is a local or semi-local function of the density.

According to Gauss's Law, Electrostatic potential, V follows the following Poisson's equation, where ρ and ϵ describes charge density and electric permittivity respectively in spatial region of the device. In our device, ϵ is only a function of z axis, so the three dimensional equation minimizes to,

$$\epsilon\left[\frac{d^2}{dx^2} + \frac{d^2}{dy^2} + \frac{d^2}{dz^2} + \frac{1}{\epsilon(z)}\frac{d\epsilon(z)}{dz}\frac{d}{dz}\right]V(x,y,z) = \frac{-\rho(x,y,z)}{\epsilon(z)} \quad (10)$$

Here multigrid finite difference algorithm is used to solve the Poisson's equation.

Transmission Coefficient:

After obtaining the self-consistent non-equilibrium density matrix, it is possible to calculate various transport properties of the system. One of the most significant of them is transmission spectrum from which the current and differential conductance can be calculated.

Here, transmission amplitude t_k defines the fraction of a scattering state of k which propagates through a device. The transmission coefficient at energy is obtained by summing up the transmission from all the states at this energy. The transmission coefficient may be obtained from the retarded Green's function using:

$$T(\varepsilon) = G(\varepsilon)(\varepsilon)G^{\dagger}\Gamma^{R}(\varepsilon) \tag{11}$$

The Electric Current:

Once the Transmission Spectrum is calculated, it is easier to calculate the current for different electrode temperatures. The current is calculated from the transmission coefficient using:

$$I(V_L, V_R, T_L, T_R) = \frac{e}{h}\Sigma_{\sigma}\int T_{\sigma}(E)[f(\frac{E-\mu_L}{k_B T_R}) - f(\frac{E-\mu_L}{k_B T_L})]dE \tag{12}$$

where f is the Fermi function, $T_{L/R}$ is the electron temperatures of the right/left electrode and $T_{\sigma}(E)$ is the transmission coefficient for the spin component .

Differential Conductance:

The differential conductance is calculated from the transmission spectrum u sing:

$$\sigma(V_l, V_R, T_L, T_R, \alpha_L, \alpha_R) = \lim_{\delta V \to \infty}(\frac{I(V_L, \alpha_L\delta_L, V_R - \alpha_R\delta V, T_L, T_R)}{\delta V}) \tag{13}$$

The coupling constant $\alpha_L + \alpha_R = 1.0$ models how the transmission spectrum couples with the left and right electrode.

Ab-initio study of absorbing H_2O molecule on semiconducting GNR:

Ab initio method is a way of quantitative calculation to predict the electronic structure and ionic dynamics. Here we have acknowledge the electron-electron interaction. First step of the calculation process is to take the Born-Oppenheimer Hamiltonian for electron [Eq.6] assuming the ions as classical components and fixed in space. These ions create an external potential field in which the electrons move. Electronic and nuclear motions are treated separately. Thus electronic structure calculation if performed for a fixed nuclear configuration by approximately After calculating the Schrodinger equation for the Born-Oppenheimer Hamiltonian, we get,

$$H_{BO}(\{r_i\};\{R_i\})\psi(\{r_i\};\{R_i\}) = E(\{R_i\})\psi(\{r_i\};\{R_i\}) \qquad (14.1)$$

This is a wave function dependent on the positions of the ions. $E(\{R_i\})$ represents the energy of the system, $\psi(\{r_i\};\{R_i\})$ represents every interactions, electron-electron and electron-ion interaction. Kinetic energy is ignored as we considered the particles to be fixed. This electronic wave function is represented in certain finite basis sets. The Schrodinger equation is then turned into an algebraic equation which can be solved through numerical methods.

There are two methods of approximations: one concerning the choice of basis functions to represent the one-electron functions called *molecular orbitals.* Other concerning the choice of N-electron functions to represent the many-electron electronic wavefunctions.

Gaussian basis functions are used to approximate the molecular orbitals, since the required integrals can be calculated very quickly in this basis. The many-electron wavefunction for the molecule is represented as a linear combination of antisymmetrized product known as *Slater*

determinants of the molecular orbitals. In full configuration interaction calculation (FCI) all possible Slater determinants for a given orbital basis are used and gives the best possible result for the chosen one-electron basis. However, the number of Slater determinants that can be constructed is enormous, and very quickly increases the number of electrons and orbitals. Therefore, approximations have to be made in which the wave function is expanded in only a subset of all possible Slater determinants.

One such approximations are used, it describes how the orbitals are determined. The most simple choice is to use a single Slater determinant and to optimize the orbital variationally. This is the *Hartree-Fock (HF) self consistent field (SCF)* method which is the initial step of ab initio calculation.

In Hartree-Fock approximation each electron moves in an average potential of the remaining electrons, but has no knowledge of the position of these. Thus , even though the Coulomb interaction between the electrons is taken into account as an average way, the electron with opposite spin are not capable of avoiding each other when they come close, and Hartree-Fock *electron correlation* method is to correct for this by taking the instantaneous correlation of the electrons into account. The corresponding energy lowering is called electron correlation energy. Density functional theory (DFT) methods can be considered to implement the electron correlation.

The Adsorption energy:

Modelling atomic adsorption by change in local effective potential using ab-initio study and tight binding hopping parameter. The adsorption energy is the energy of the isolated graphene sheet and isolated molecule minus the energy of the fully relaxed graphene sheet with the molecule adsorbed to it [9]. It is calculated as

$$E_{ads} = E_{GNR+mH20} - (E_{GNR} + mE_{H20}\ ) \tag{14.2}$$

Where $E_{GNR+mH20}$ is the total energy of GNR with an absorbed H_2O molecule. E_{GNR} and E_{H20} are the total energies of pristine GNR (semiconducting or metallic) and isolated H_2O molecule respectively and m is the number of absorbed H_2O molecule. The adsorption energy is a required parameter to understand the electronic properties and how strong the interaction occurs among the molecules. Higher adsorption energy represents high interaction between the the adsorbate and adsorbed molecule.

Device Configuration

In this paper four types of Graphene Nanoribbon FETs are proposed all of them having Armchair chirality. The types are differed on the basis of changes in channel and source-drain region shown in Fig.3-6. For cascaded Metallic-Semiconducting-Metallic device in Fig.3, N=7 (E^g = 1.35eV) semiconducting Armchair nanoribbon of 3.5nm channel length, where N describes the number of carbon atoms along the width of armchair GNR. This region is connected with N=8 (E^g = 0eV) metallic armchair nanoribbons considered as electrodes having the width of ~0.74nm. Fig. 4, 5 devices are respectively made of solely metallic GNR (N=11) and semiconducting GNR (N=7). Lastly, Fig.6 has a top gated channel of cascade metallic (N=8) - semiconducting (N=7) –metallic (N=8). The detailed behavior and transport properties of these devices will be discussed in the subsequent chapter.

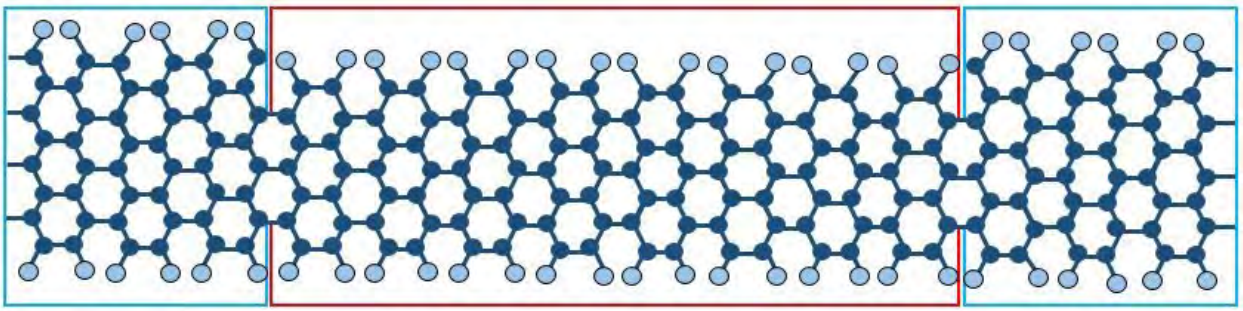

Fig.3 : Metallic(N=8)-Semiconducting(N=7)-Metallic(N=8)

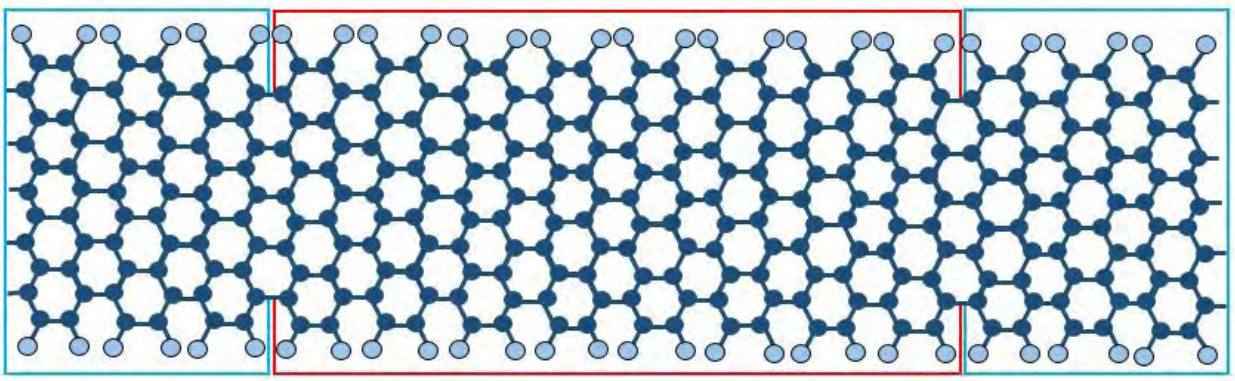

Fig.4: Metallic(N=11)-Metallic(N=11)-Metallic(N=11)

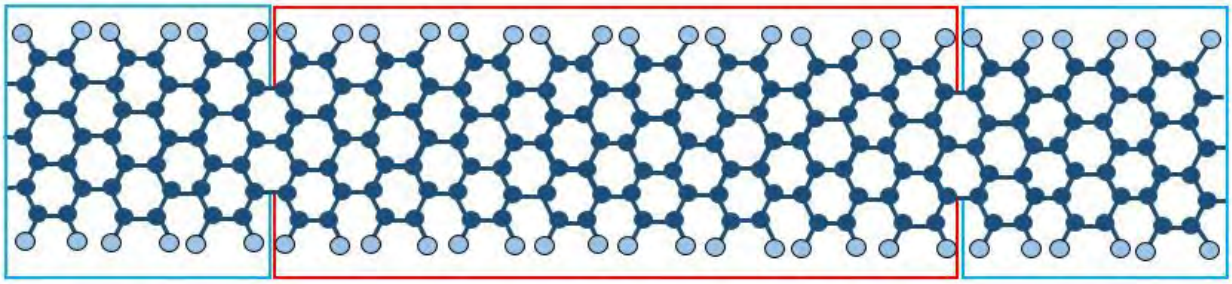

Fig.5: Semiconducting(N=7)-Semiconducting(N=7)-Semiconducting(N=7)

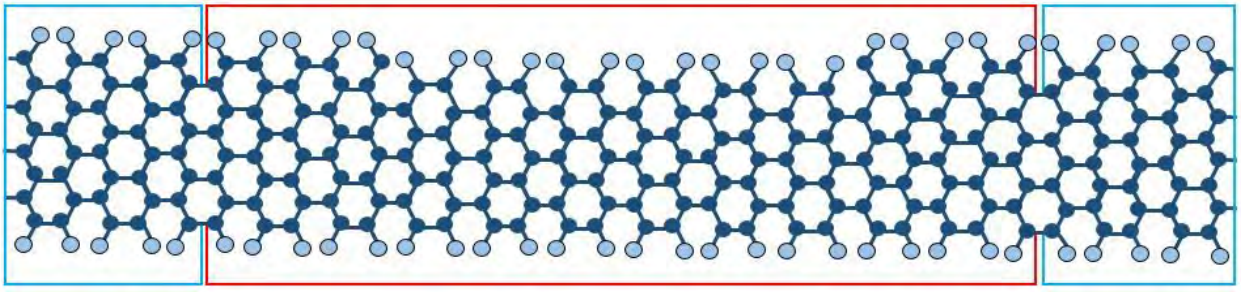

Fig.6: Cascaded (Metallic(N=8)-Semiconducting(N=7))

Results

Transport properties:

According to the cascaded Metallic-Semiconducting-Metallic fig.3 devices, it has a correlation of Metallic- Semiconducting- Metallic where the semiconducting Armchair Nanoribbon (N=7, E(G) = 1.35eV) has been used as a channel along with two metallic armchair nanoribbon (N=8, E(G) = 0eV) as the electrodes in the device. This cascading structure provides a remarkable combination between channel and electrodes which in case, reduces the possibility of occurring the impurity scattering and interface defects. Instead of using metallic armchair GNR, if we used a contact metal that would give us a large amount of contact resistance; but as we used the metallic armchair GNR, it reduces that fact and introduces a smoother interface with a minimum amount of contact resistance which makes the \cascaded Metallic-Semiconducting-Metallic fig.3 devices more efficient[7].

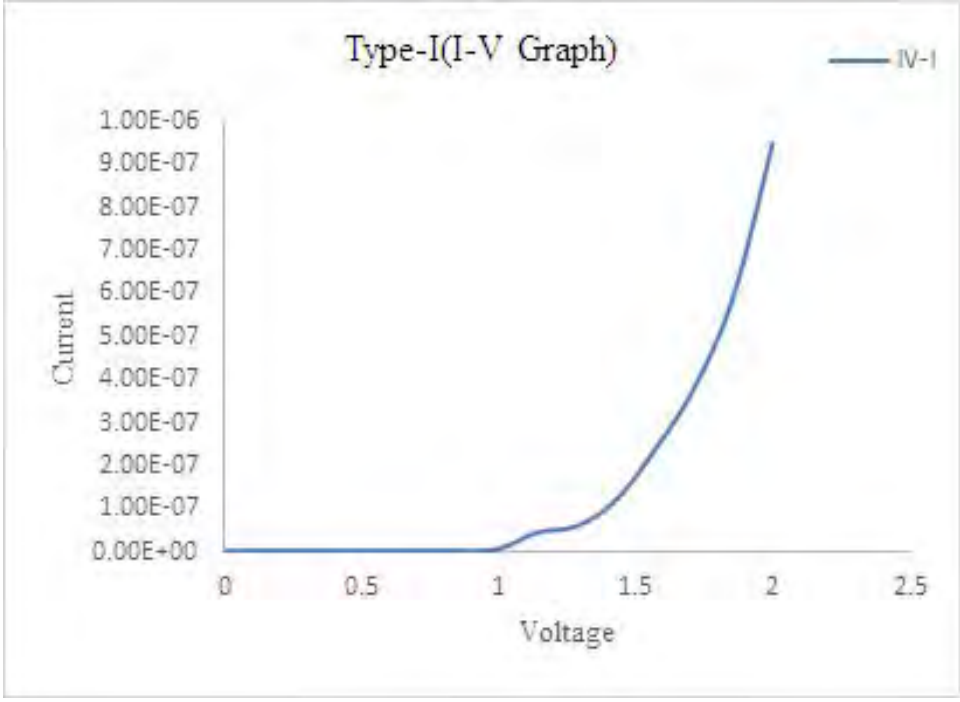

Fig.7(a): cascaded Metallic-Semiconducting-Metallic (*I-V* curve) at zero gate voltage

For cascaded Metallic-Semiconducting-Metallic fig.3 bias voltage of drain-source and the gate voltage have the greater impact than the other three types of devices on the current at the channel region[7]. In case of applying positive potential , we have increment characteristic for the drain-source current behavior as the minimum energy for non zero electron transmission coefficient comes closer to fermi energy level proved in previous works[7] .

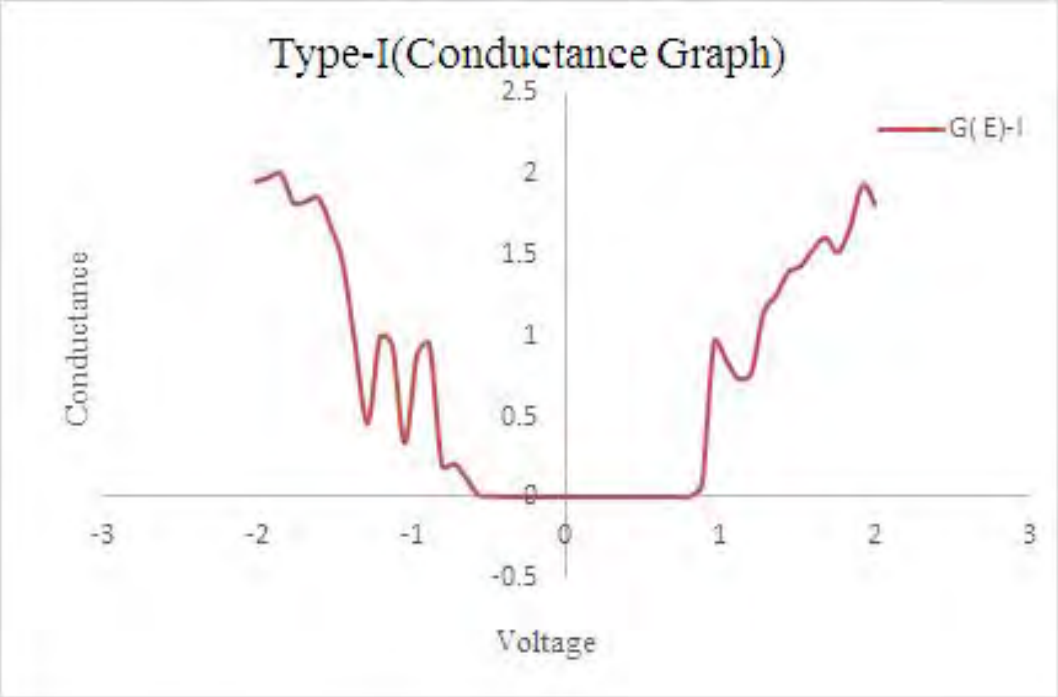

Fig.7(b): cascaded Metallic-Semiconducting-Metallic conductance at zero gate voltage

From *I-V* fig.7(a) curve of cascaded Metallic-Semiconducting-Metallic device we can see that upto 0V~1V there is no change at the graph but after 1V current increases . Therefore, this behavior conforms the conductance graph fig.7(b) that it shows no changes at 0V to approximate 1V and after crossing 1V conductance increases drastically.

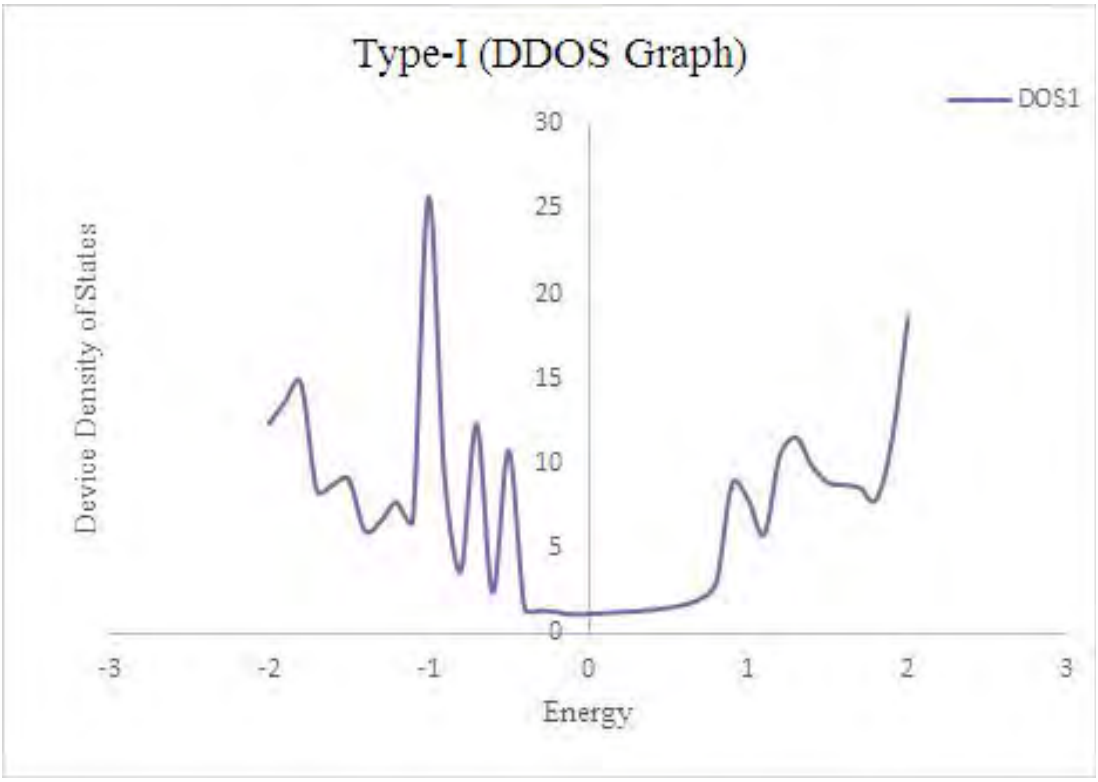

Fig.7(c): cascaded Metallic-Semiconducting-Metallic Device Density of State graph at zero gate voltage

This DOS fig.7(c) graph shows a sharp peak at lower energy below Fermi level for zero gate voltage in the valence band and clearly indicates the pattern of a FET behavior. Moreover, there is small changes at peaks above the fermi level in the conduction band which also indicates better performance for cascaded Metallic-Semiconducting-Metallic fig.3 as a field effect transistor including the conductance and *I-V* characteristics.

Metallic-Metallic-Metallic fig.4 is another combination of GNR, exclusively made of Metallic GNR (N = 11). From the figure, Metallic-Metallic-Metallic fig.4 describes zero band gap that confirms the metallic behavior of Metallic-Metallic-Metallic devices where a very high current

can get produced by a small bias voltage but upon this voltage it provides a less impact of top-gate voltage[7]. The current-voltage characteristics gained from Metallic-Metallic-Metallic devices are like resistor type behavior with resistance in K-Ohm range. It means, it can perform as a better interconnect[6].

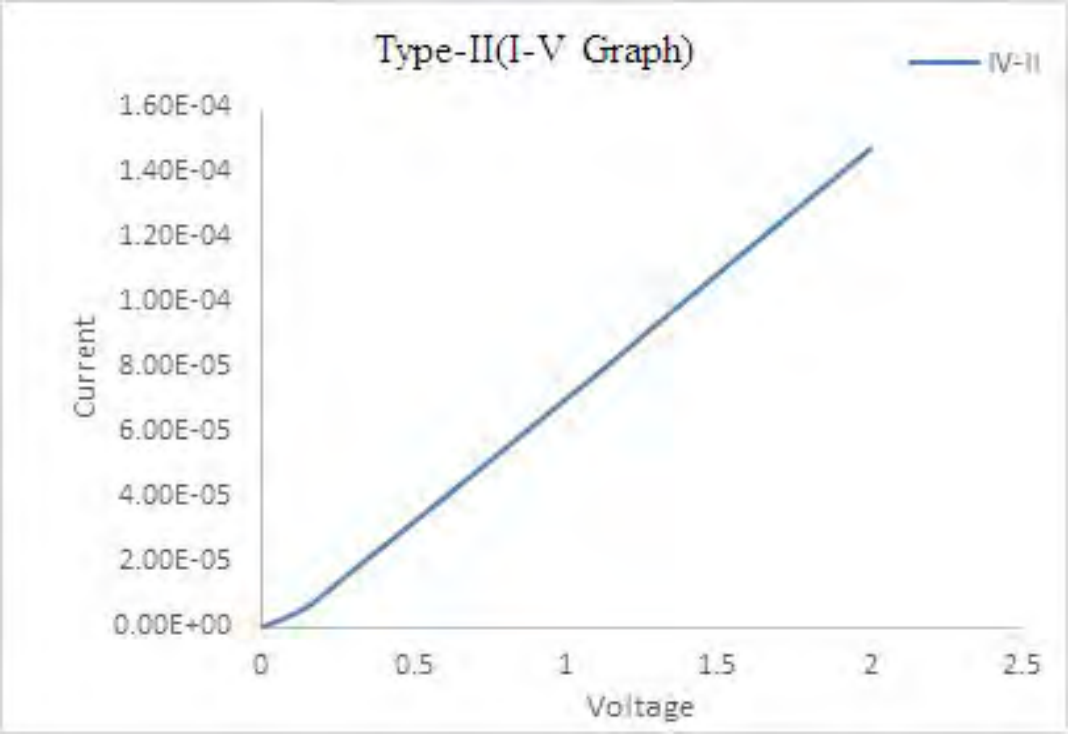

Fig.8(a): Metallic-Metallic-Metallic (*I-V* curve) at zero gate voltage

Metallic-Metallic-Metallic fig.4 I-V curve fig.8(a) shows linearity means current and voltage changes proportionally with a larger amount of resistance as previously proved[7].

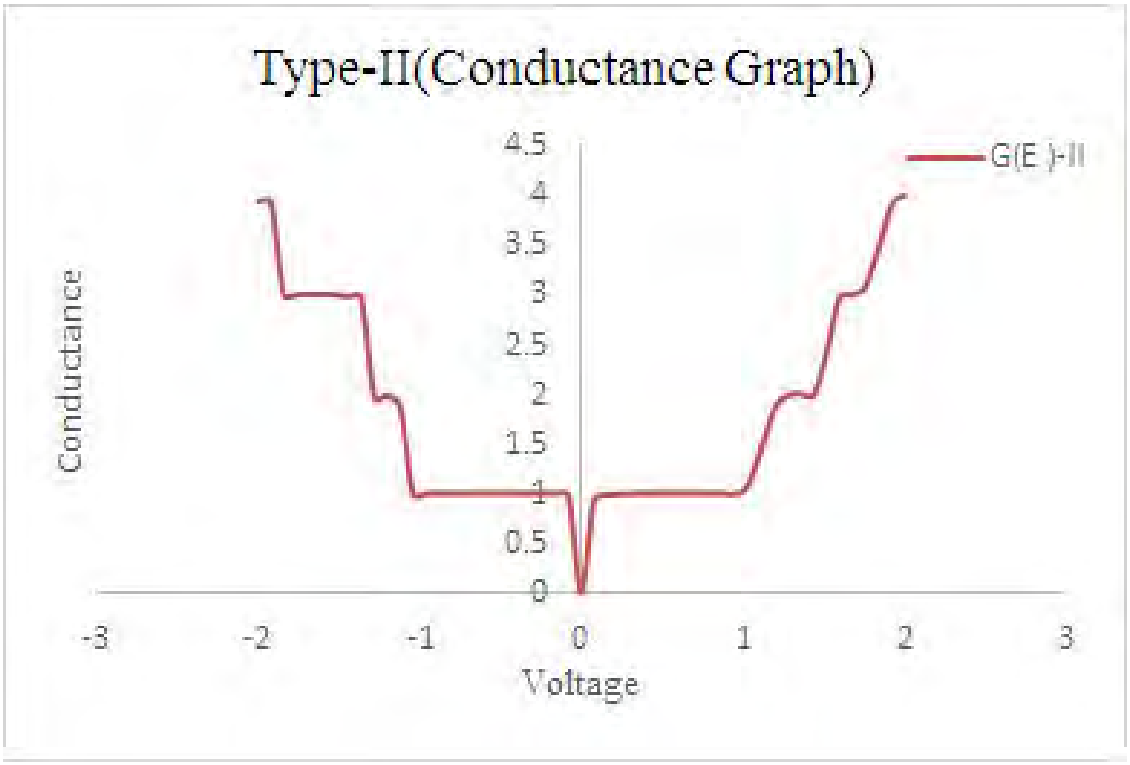

Fig.8(b): Metallic-Metallic-Metallic conductance at zero gate voltage

Therefore, the conductance graph fig.8(b) linear increment behavior where conductance increase as the voltage increases. From DOS fig.8(c) graph of Metallic-Metallic-Metallic , we can exhibit a large peak appears above the Fermi level that proves that the system is strongly metallic with the increment of significant conductivity.

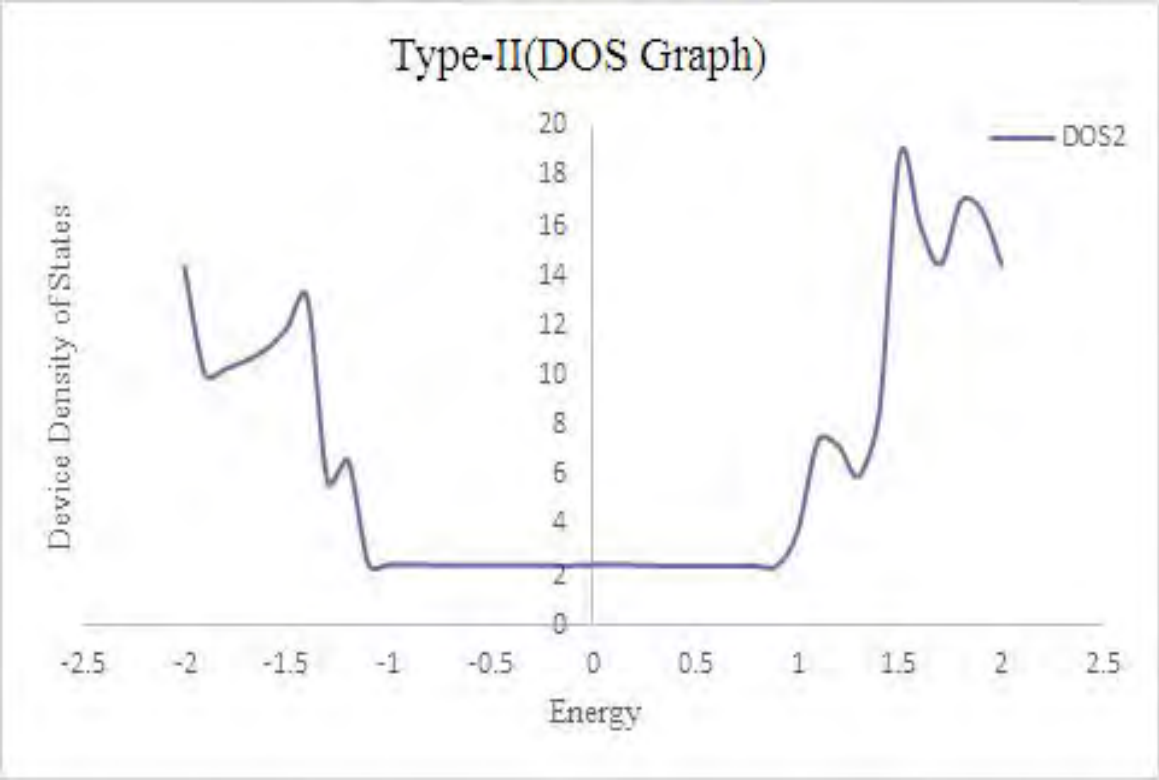

Fig.8(c): Metallic-Metallic-Metallic Device Density of State graph at zero gate voltage

Semiconducting-Semiconducting-Semiconducting fig.5 devices shows the combination of a Semiconducting GNR (N = 7). From the transmission spectrum of Semiconducting-Semiconducting - Semiconducting devices it is retrieved as a 2D semiconductor (fig), But due to having schottky barrier and a high amount of contact resistance, the current fig.9 (a) may get demoted a lot due its relatively high band gap[7].

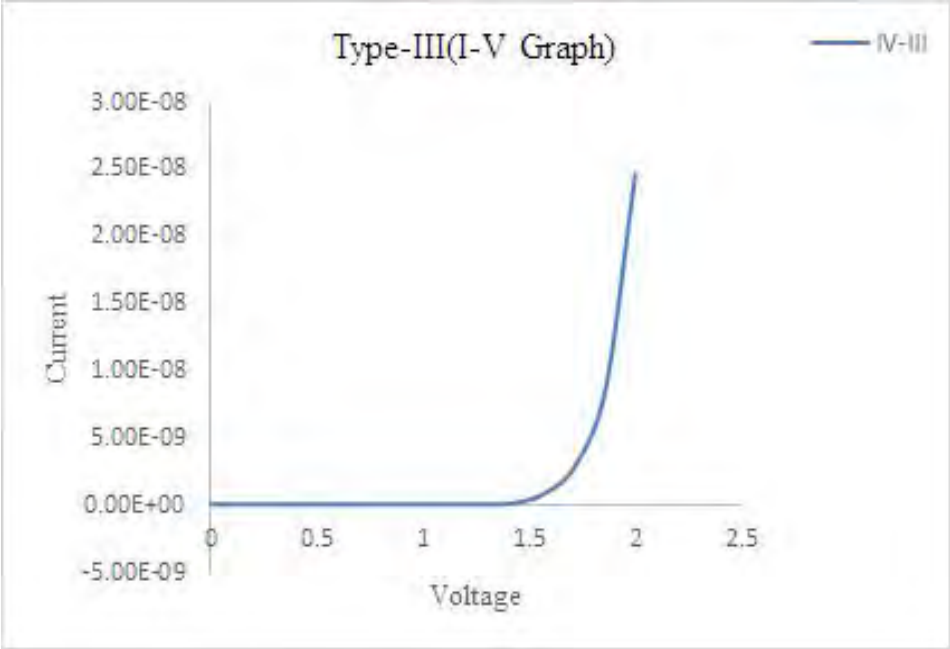

Fig.9(a): Semiconducting-Semiconducting-Semiconducting (*I-V* curve) at zero gate voltage

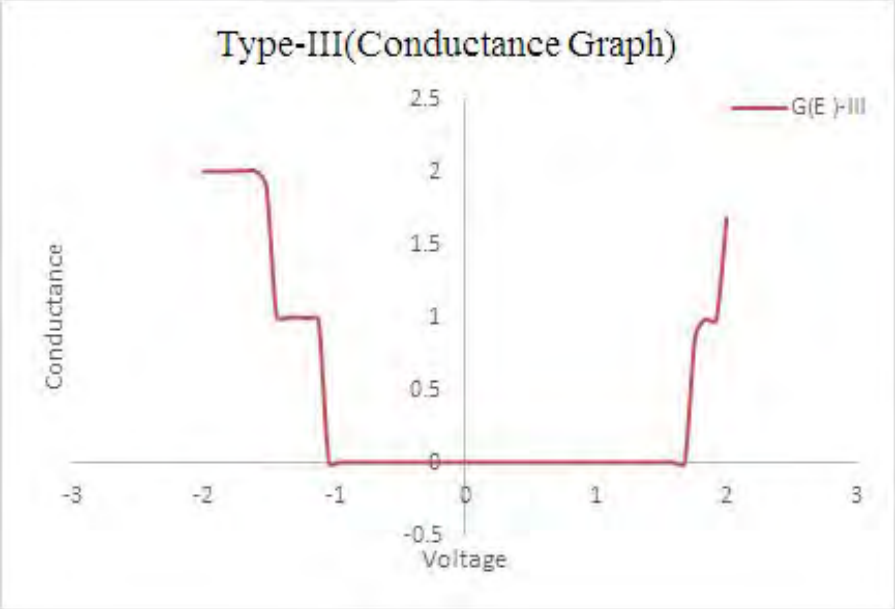

Fig.9(b): Semiconducting-Semiconducting-Semiconducting conductance at zero gate voltage

DOS fig.9(c) graph shows clear drop at the Fermi level which indicates the behavior of a semiconductor. There is no conductance till 1.5V as it has high bandgap.

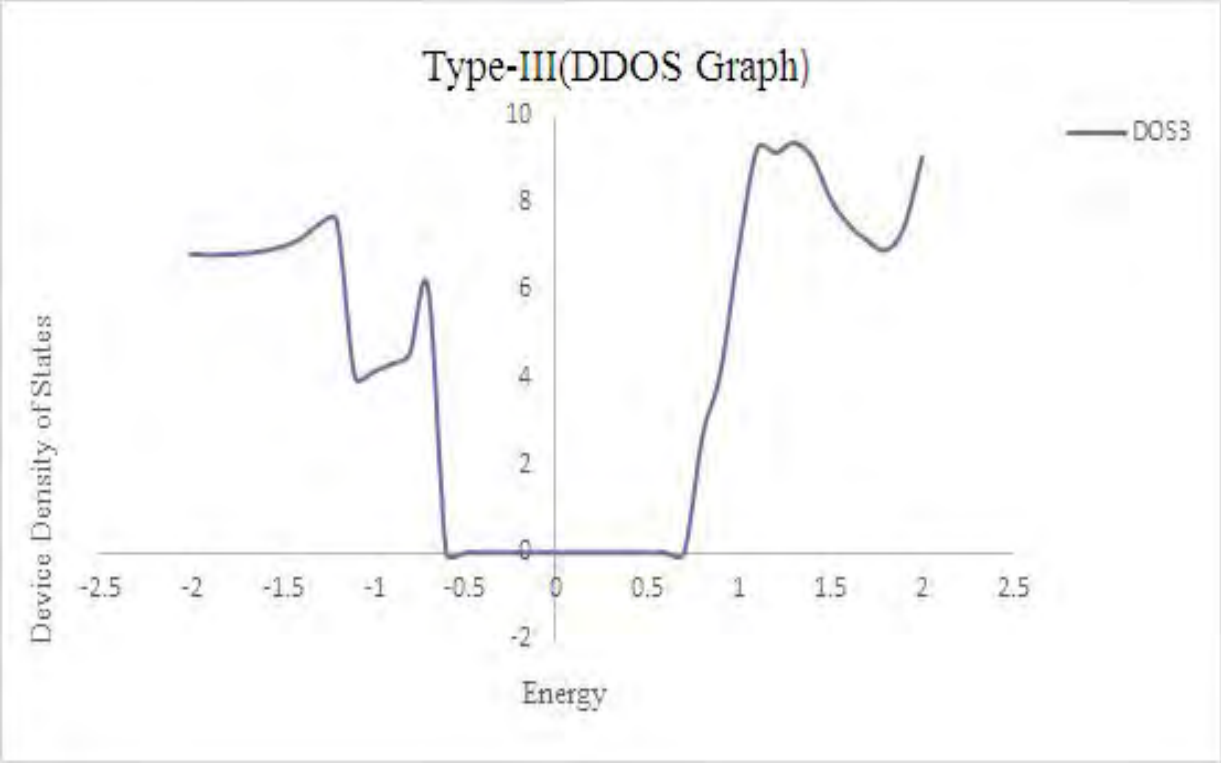

Fig.9(c): Semiconducting-Semiconducting-Semiconducting Device Density of State. graph at zero gate voltage

cascaded Metallic-(Metallic+Semiconducting+Metallic)-Metallic fig.6 is basically cascaded version of Metallic-Metallic-Metallic and Semiconducting-Semiconducting-Semiconducting where at contact metallic armchair GNR and at channel both semiconducting and metallic armchair GNR have been used. For the cascaded hetero armchair GNR has increment of conduction region which is the result of putting vacancies on effective channel. As the local energy states are being inserted to the conduction region, current may show increment characteristic as well. Lower bias voltage can be the source for getting significant conductance for cascaded armchair GNR than metallic or semiconducting GNR. When E=0 it shows the fermi energy without even having external bias voltage. The conduction is zero in the bandgap region as there is no energy state of unadsorbed cascaded GNR which reflects the characteristics of

difference among sheet potentials on three different directions and their potential is zero along the transportation direction towards the length of GNR[4]. Cascaded GNR creates potential barrier for electrons which increase the quasi quantized energy states[4]. Therefore, these potential barriers are the reason why conduction increases and as result of increasing the current at a point. Cascaded hetero GNR is the mixer of semiconducting armchair GNR and the metallic armchair GNR on characteristics. cascaded Metallic-(Metallic+ Semiconducting+Metallic) -Metallic, cascaded armchair GNR can work even at lower voltage where the only thing we can notice that it may show some fluctuates as it performs both semiconducting armchair GNR and metallic armchair GNR[] . Here, for metallic region transmission coefficient is nonzero where is the band gap region of semiconducting GNR [7]. This characteristic shows the resistance behavior which may be controlled by the top gate voltage[6]. Moreover, we can get different resistance in mega ohm range by only varying the length of semiconducting armchair GNR or the metallic armchair GNR. As a result we can use this type as on-chip resistance in industry[7].

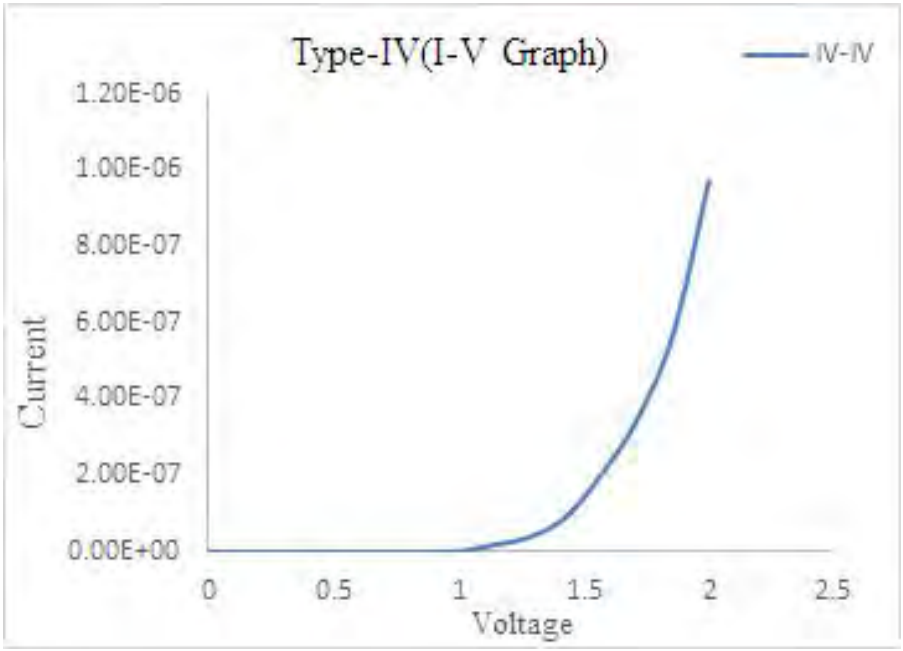

Fig.10(a): cascaded Metallic-(Metallic+Semiconducting+Metallic)-Metallic (*I-V* curve) at zero gate voltage

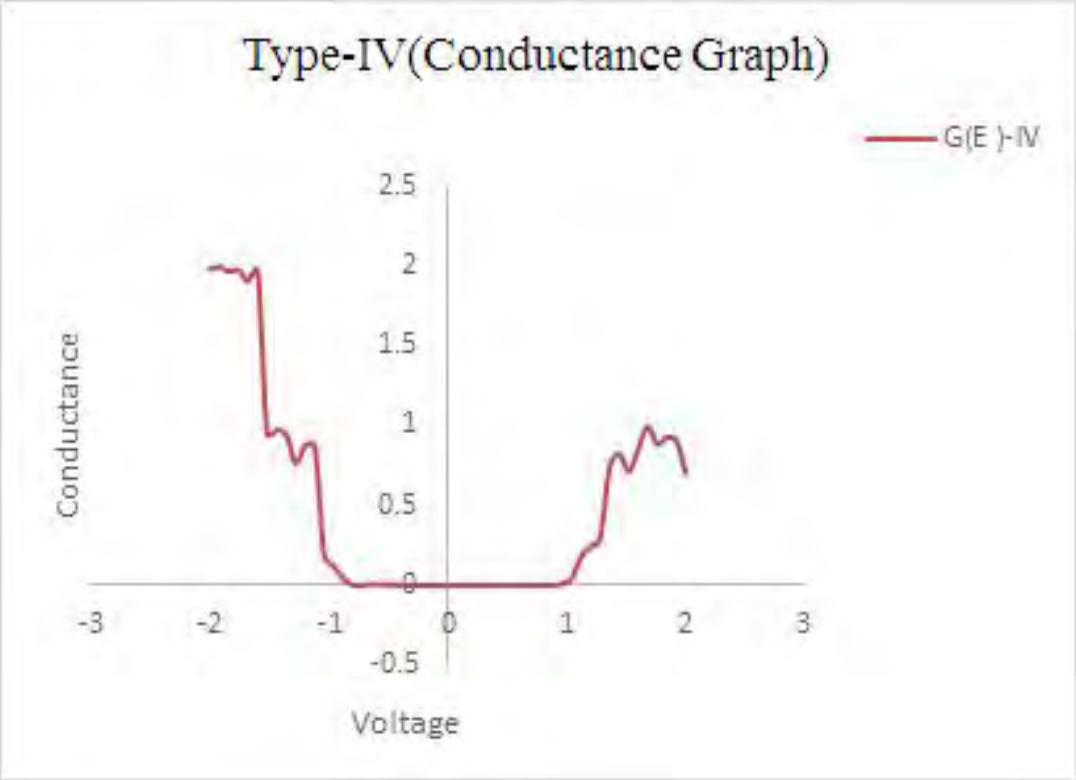

Fig.10(b): cascaded Metallic-(Metallic+Semiconducting+Metallic)-Metallic conductance at zero gate voltage

DOS fig.10(c) and conductance fig.10(b) graph for cascaded Metallic-(Metallic+Semiconducting +Metallic)-Metallic fig.6 show both semiconducting and metallic behavior as we have used both semiconducting and metallic armchair GNR at channel. As a result we can see that conductance is Zero upto 1V and then increases for conductance graph fig.10(b). On the other, hand we can see sharp peaks both below and above of the Fermi level for DOS graph fig.10(c). Since, it shows both metallic and semiconducting behavior, as a matter of fact it is controllable which means we can change its characteristics behavior by changing either the metallic armchair GNR or the semiconducting armchair GNR.

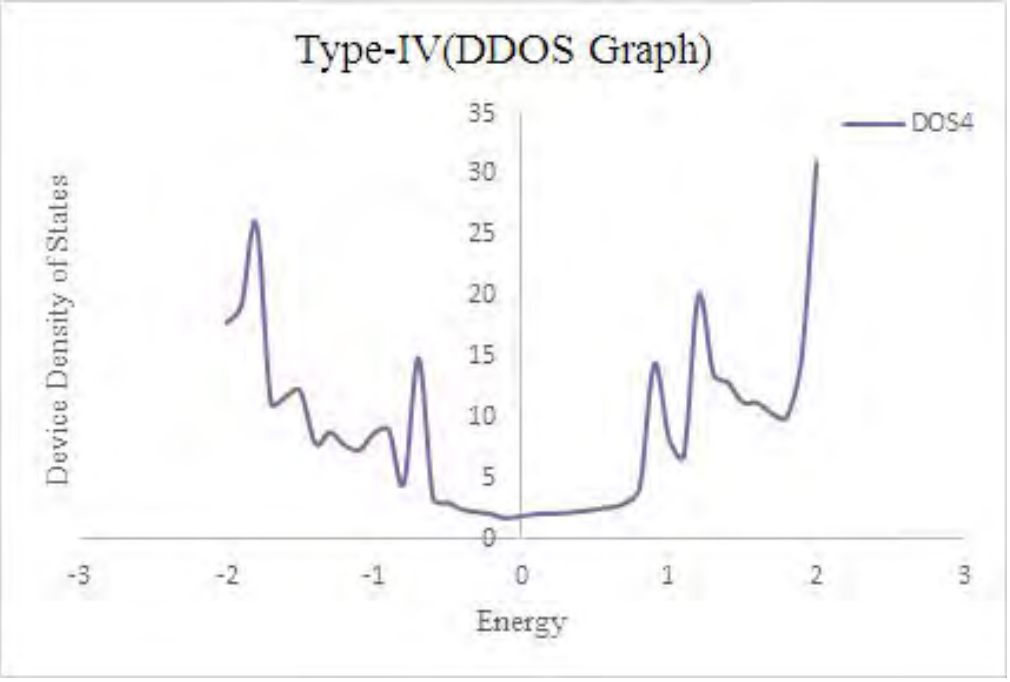

Fig.10(c): cascaded Metallic-(Metallic+Semiconducting+Metallic)-Metallic Device Density of State graph at zero gate voltage

Implementation

From the graph Fig.11(a) we can say that we are comparing cascaded Metallic-Semiconducting-Metallic fig.3 and cascaded Metallic-(Metallic+Semiconducting+ Metallic)-Metallic fig.6 to create a device, In some previous work we have found out inverter is the perfect choice from these two devices where there *I-V* characteristic was the only key.

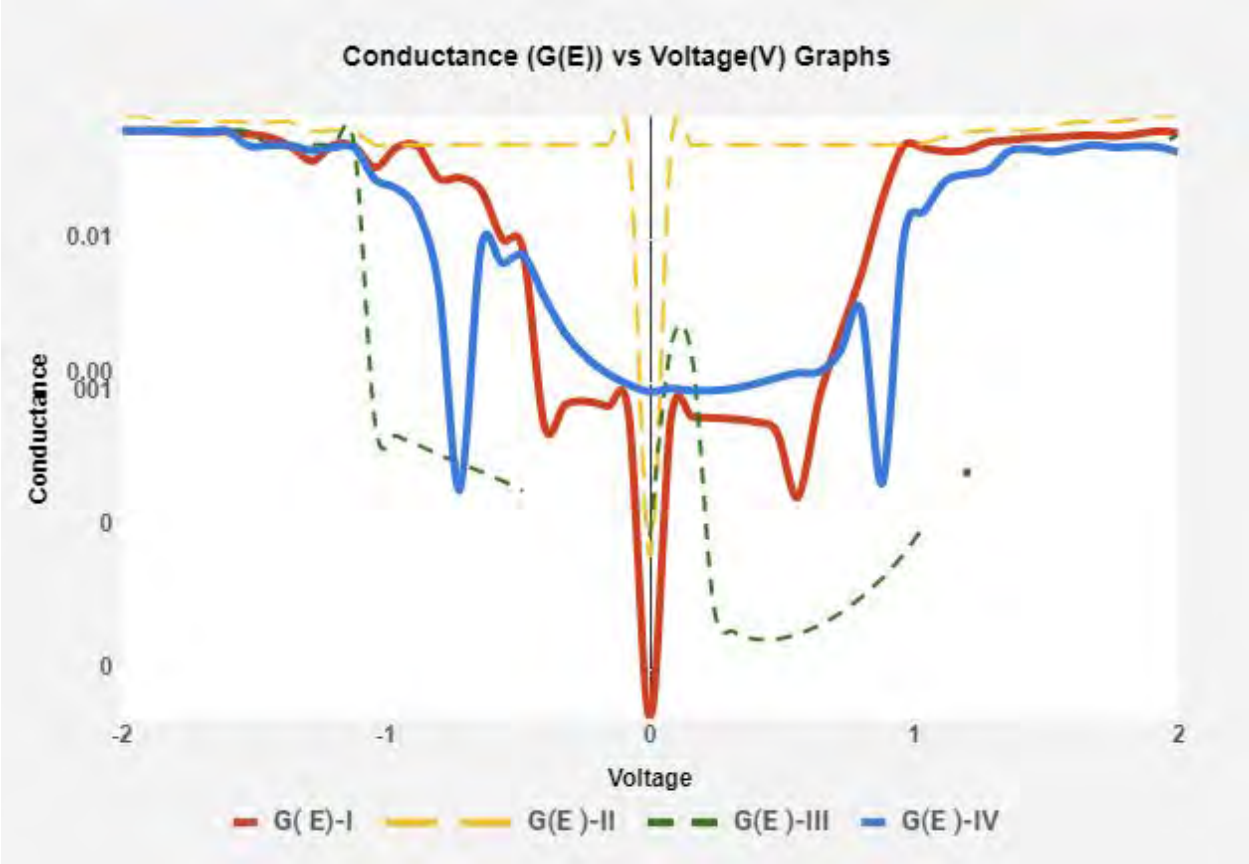

Fig.11(a): Conductance vs Voltage graph for four types devices

From fig,11(a) it gives the clear theory for being the perfect match. Here, at 0V~1V cascaded Metallic-Semiconducting-Metallic and Metallic-Metallic-Metallic shows zero conductance. When voltage increases from 1V cascaded Metallic-Semiconducting-Metallic shows increasing conductance behavior and cascaded Metallic-(Metallic+Semiconducting+Metallic)-Metallic shows decreasing behavior (a sharp peak at the opposite direction of cascaded Metallic-Semiconducting-Metallic fig.11(a)) . Whereas, it was the actual inverting behavior for our considered inverter, previously which showed only by the *I-V* curve behavior[7] but this proof makes the statement much stronger.

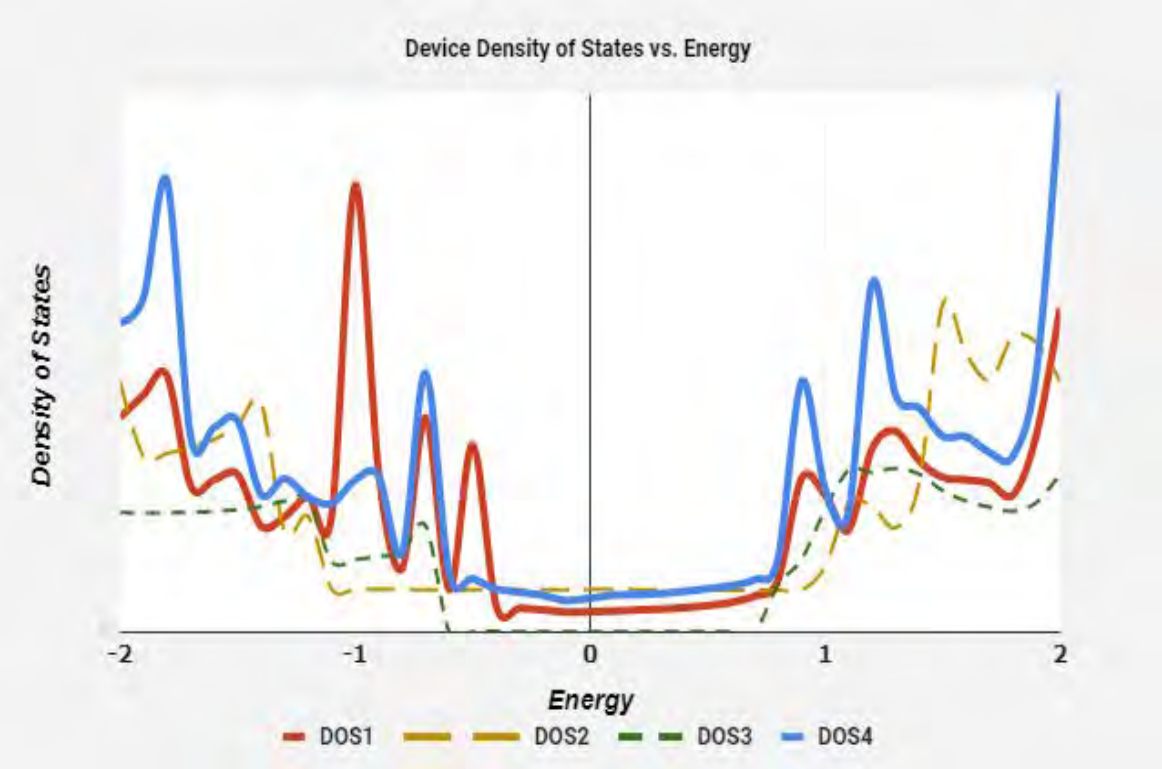

Fig.11(b): Device Density of State vs Energy Graph for four types considered Devices

For fig.11(b) Device Density of States shows the ultimate result with more reasonable conditions.From this compared graph we spectating that cascaded Metallic-Semiconducting-Metallic DDOS fig.11(b) has the sharp peak below fermi level which makes it work as a perfect

FET. On the other hand, cascaded Metallic-(Metallic+Semiconducting+Metallic)-Metallic has sharp peaks in both sides of the fermi level as it has both semiconducting and metallic AGNR at the channel. At previous work it was proved that we can change cascaded Metallic-(Metallic+Semiconducting+Metallic)-Metallic either semiconducting or metallic[7] which is exactly being the proved by this DDOS graph fig.11(b) to make it clear that we are more capable to have the structure for our desired device. Where we considered Metallic-Semiconducting-Metallic fig.3 as Type-I, Metallic-Metallic-Metallic fig.4 as Type-II, Semiconducting-Semiconducting-Semiconducting fig.5 as Type-III and Metallic-(Metallic+ Semiconducting+Metallic)-Metallic as Type-IV.

Due to the absence of current saturation, it is challenging to design a FET device from GNR with respect to MOSFET [6]. But using ratioed circuit topology we can propose a logical device structure. From the previous discussion, it is obvious that cascaded Metallic-Semiconducting -Metallic device is appropriate to use as pull-up network due to its perfect Field Effect Transistor behavior. Whereas, cascaded Metallic-(Metallic+Semiconducting+Metallic)-Metallic can be used as a suitable pull-down network due to high resistance and flexibility.

Metallic-Metallic-Metallic fig.4 shows pure metallic character. As conductance graph fig.8(b) and DDOS graph fig.8(c) show that it has perfect conductance with linearity and it has sharp peaks above the fermi level means at the valence band, therefore it is perfect for having metallic character. Because of its metallic behavior we can use Metallic-Metallic-Metallic fig.4 as the interconnect between the cascaded Metallic-Semiconducting-Metallic and cascaded Metallic -(Metallic+Semiconducting+Metallic)-Metallic to make the inverter work more efficiently.

Below we proposed an inverter configuration at fig.12 where cascaded Metallic-Semiconducting -Metallic fig.3 working as the input voltage and cascaded Metallic-(Metallic+Semiconducting +Metallic)-Metallic fig.6 gate is connected to to ground as it shows opposite characteristics from cascaded Metallic-Semiconducting-Metallic fig.3. Interconnection for two types is Metallic-Metallic-Metallic fig.4 and we can have the output through this connection. Bias

voltage is 1V because the properties DDOS fig.7(c) & fig.10(c), conductance fig.7(b) & fig.10(b) for both cascaded Metallic-Semiconducting-Metallic and cascaded Metallic-(Metallic+ Semiconducting+ Metallic)-Metallic shows particular capabilities from 1V.

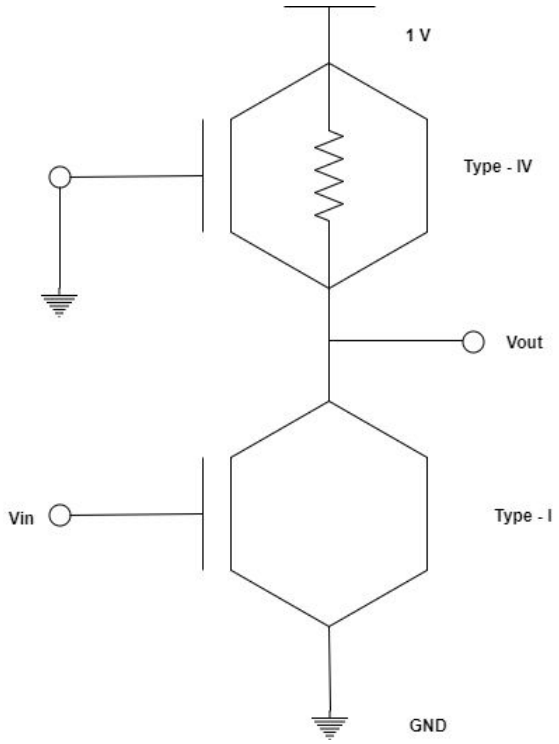

Fig.12 : Inverter using cascaded Metallic-Semiconducting-Metallic and cascaded Metallic-(Metallic+Semiconducting+Metallic)-Metallic devices

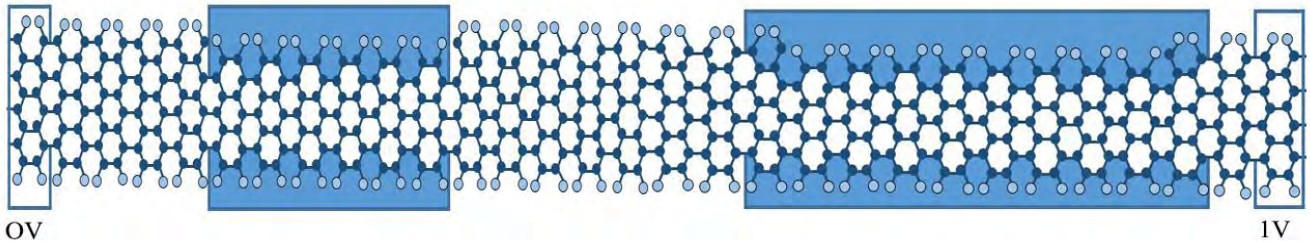

Fig.13 : Layout diagram of a GNR inverter [at left Type-I, middle Type-II and at the right Type-IV]

Sensing Properties

Graphene is a 2D material with a surface with almost no volume, which causes the maximization of the effect of surface dopants [8]. It was also shown that if gas molecules were adsorbed on the graphene surface, the charge carrier concentration of graphene was increased [9]. So the adsorbed graphene can be used as a highly sensitive sensors even with the possibility of detecting individual molecules[8]. The sensor property is based on the changes in resistivity due to molecules adsorbed on graphene that act like donors or acceptors.

From a previous study on vapor (H_2O)adsorption on armchair GNR, where the adsorption process only occur to the π electrons of GNR and the electrons oxygen ion in H_2O [14].

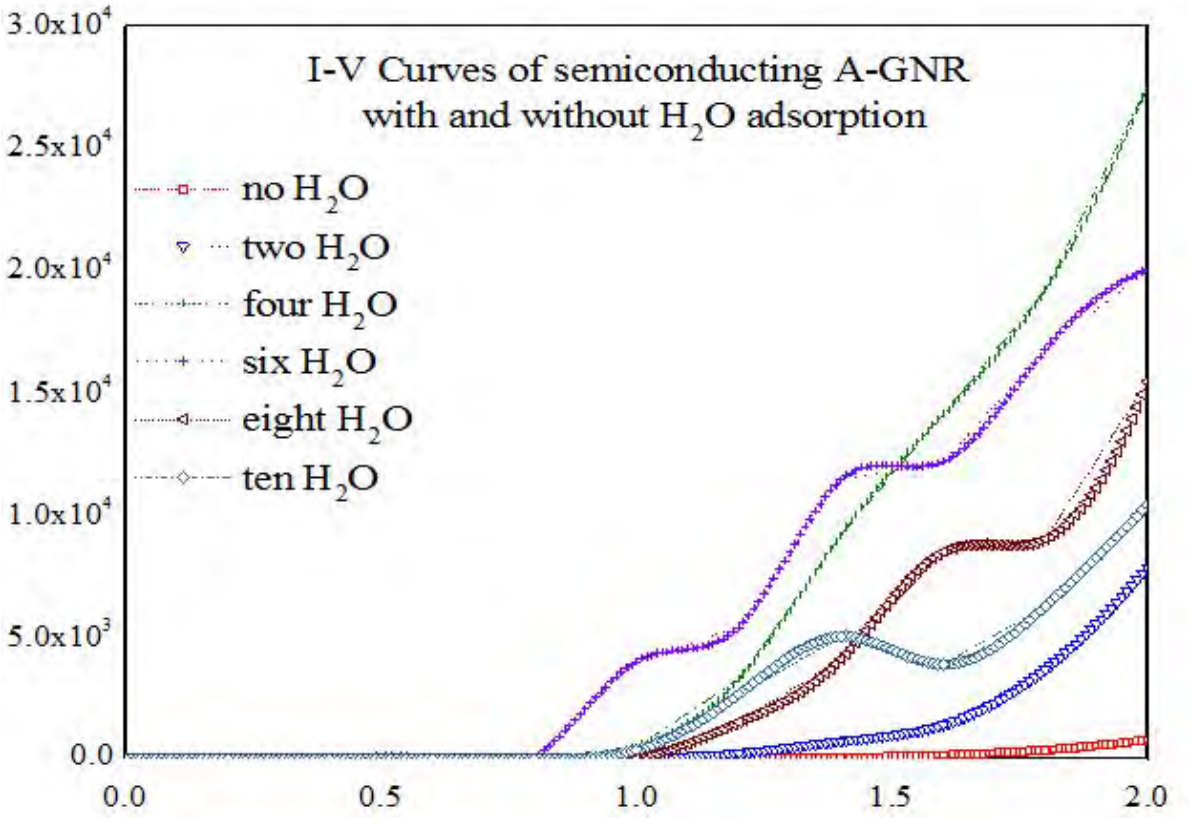

Fig. 14 (a): *I-V* Curves of semiconducting A-GNR with and without H_2O adsorption [14]

Fig.11(c) shows the simulated current voltage characteristics of semiconducting A-GNR. Typically this configuration does not show significant conduction below 0.75V and then its conduction increases with the increment of bias voltage V_b , whereas adsorption of H_2O increases the current more significantly depending on number of absorbed water molecule[14]. Interestingly, after six H_2O molecules, current started to decrease with the increment of molecules. Then the conduction also decreases with the increment of bias voltage.

But in this experiment the ab initio method was not introduced and the molecular orientation and the adsorption site of GNR has not been considered yet. So in our experiment, we simulated the adsorption process using ab initio method. Next, we have considered three different adsorption site, the center part of the carbon hexagon (C), top of carbon atom (T), and the middle point of the C-C bond (B). Added to that, we have analyzed three different orientation of the molecule H_2O: from O atom, O-H bonds pointing down (d), O-H bonds pointing up (u), and parallel (n) with respect to GNR surface. Then we calculated the adsorption energies for all the orientations.

We have considered the effects of adsorption over the transport properties of semiconducting (N=7)-semiconducting(N=7)-semiconducting (N=7) , where semiconducting GNR is the channel acting as a sensing medium.

If the Highest Occupied Molecular Orbital (HOMO) is above the Fermi level of graphene, the charge transfer occurs from the adsorbate to GNR, and if the Lowest Occupied Molecular Orbital (LUMO) is below the Fermi level, charge transfer will take place from GNR to adsorbate.

Table 1: The adsorption energy is determined by the orientation of adsorbate (u= pointing up, d= pointing down and n= pointing parallel) and adsorption sites (C= center of carbon hexagonal, T= top of carbon atom and B= the center point of C-C bond)

Position	Orientation	adsorption Energy E_g (eV)
C	u	-2.20
C	d	-1.40
C	n	-1.60
T	d	-2.34
T	u	-2.13
T	n	-1.86
B	d	-2.38
B	u	-2.40
B	u	-1.80

All the properties and adsorption energy seem to be almost independent of the adsorption sites but from Table 1 we can see that the center part of the carbon hexagon of semiconducting GNR is shown to be the most interactive with H_2O molecule in order to get the highest binding energy. At the center region, when O atom points to the GNR surface, there is a significance charge transfer. On the other hand, if the H atom points to the GNR surface, there is a less amount of charge transfer to H_2O molecule.

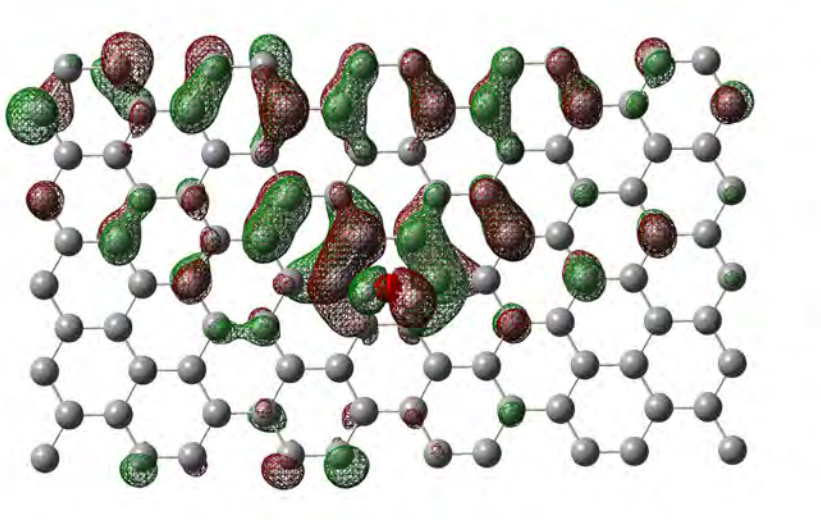

Fig.14(b): Highest Occupied Molecular Orbital (HOMO)

the type 3

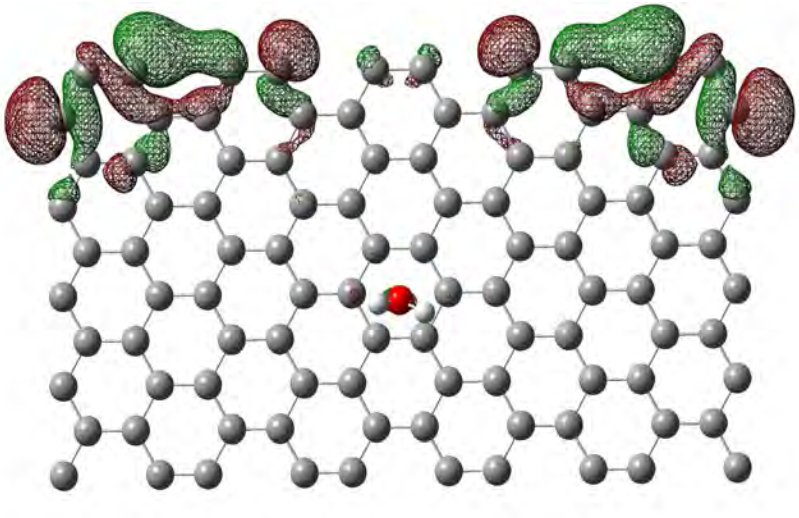

Fig.14(c): Lowest Unoccupied Molecular Orbital (LUMO)

Notably, formation of HOMO and LUMO of H_2O molecules and their orientations play an important role in charge transfer mechanism. It is found that HOMO is located mostly on the O atom where LUMO is mostly located on the H atom. A small mixing of the orbital between absorbates and GNR above Fermi level is found in pointing up parallel direction, which causes a

charge transfer to GNR from adsorbates. However, there is also a stronger mixing with the orbital below the Dirac points as they are close to energy level but this does not induce any charge transfer because there is no vacancy.

In pointing down direction, a strong interaction has occured between the surface of GNR and the LUMO of the adsorbates below Dirac point as a result some charge is transferred to H_2O molecule from GNR due to mixing of the orbitals. However, there is a strong interaction in orbital above the Dirac point, but this does not induce any charge transfer as all the orbitals are empty above Fermi level.

Again, in pointing parallel direction, there is a strong interaction in HOMO but at the same time, there will almost same interaction in LUMO. There will be a charge transfer from the H_2O molecule to GNR, but, because of the interaction with the LUMO, it will be smaller. However, we focus only semiconducting A-GNR as we have found that in case of metallic GNR, the adsorption effect have a smaller impact over modifying the electronic properties.

Conclusion

To conclude, we first discussed the electronic structure of the four types of patterned armchair graphene nanoribbon devices. Then we simulated their quantum transport properties such as current-voltage characteristics, conductance, device density of states using density Functional theory (DFT) along with non equilibrium green's function (NEGF) formalism. By analyzing the transport properties, we have gathered that Type-I devices have the potential to be high performing FET. While Type-II devices can be chosen as interconnect for it's metallic properties, Type-IV act better as on chip resistance. Then we proposed a model of a logical inverter articulated from the simulation. After that, we observed the H_2O molecular adsorption on semiconducting GNR changing the molecular orientation and adsorption site. Then we calculated the adsorption energies . The highest occupied molecular orbitals and lowest unoccupied molecular orbitals (HOMO and LUMO) were introduced to analyze their charge transport mechanism to examine whether the sensor properties can be improved. We expect that our simulated device structure will lead to further useful applications in the field of material science and carbon-based technology.

Reference

[1]S. Reich, J. Maultzsch, C. Thomsen and P. Ordejón, "Tight-binding description of graphene", *Physical Review B*, vol. 66, no. 3, 2002.

[2]E. Hwang, S. Adam and S. Sarma, "Carrier Transport in Two-Dimensional Graphene Layers", *Physical Review Letters*, vol. 98, no. 18, 2007.

[3]A. Geim and K. Novoselov, "The rise of graphene", *Nature Materials*, vol. 6, no. 3, pp. 183-191, 2007.

[4]S. Shakil, N. Tarannum and M. Rhaman, "A Comparative Study of Increasing Sensitivity Based on MoS2 Gas Sensor", *Journal of Nano- and Electronic Physics*, vol. 9, no. 6, pp. 06003-1-06003-4, 2017.

[5] S. Datta, "Nanoscale device modeling: the Green's function method", *Superlattices and Microstructures*, vol. 28, no. 4, pp. 253-278, 2000.

[6] A. Saha, G. Saha and A. Rashid, "Effect of Stone-Wales Defects and Edge Roughness on The Switching and Frequency performance of Graphene Nanoribbon-FET", 2014.

[7] A. Saha, "Low Power Dissipation Logic Inverter Design Using Atomic-Level Width Controlled GNR-FETs", 2014.

[8] K. Novoselov, A. Geim, S. Morozov, S. Dubonos, Y. Zhang and D. Jiang, "Room-temperature electric field effect and carrier-type inversion in graphene films", *Nature*, 2004.

[9] F. Schedin, A. Geim, S. Morozov, E. Hill, P. Blake, M. Katsnelson and K. Novoselov, "Detection of individual gas molecules adsorbed on graphene", *Nature Materials*, vol. 6, no. 9, pp. 652-655, 2007.

[10] B. Huang, Z. Li, Z. Liu, G. Zhou, S. Hao, J. Wu, B. Gu and W. Duan, "Adsorption of Gas Molecules on Graphene Nanoribbons and Its Implication for Nanoscale Molecule Sensor", *The Journal of Physical Chemistry C*, vol. 112, no. 35, pp. 13442-13446, 2008.

[11] J. Kong, "Nanotube Molecular Wires as Chemical Sensors", *Science*, vol. 287, no. 5453, pp. 622-625, 2000.

[12] K. Novoselov, A. Geim, S. Morozov, D. Jiang, M. Katsnelson, I. Grigorieva, S. Dubonos and A. Firsov, "Two-dimensional gas of massless Dirac fermions in graphene", *Nature*, vol. 438, no. 7065, pp. 197-200, 2005.

[13] S. Shakil, F. Zohra, P. Pramanik, R. Tushar, A. Saha and M. Bhuian, "Humidity sensor using surface adsorbed channel modulated Graphene nanoribbon: NEGF approach", *8th International Conference on Electrical and Computer Engineering*, 2014.

[14] S. Shakil, F. Zohra, P. Pramanik, R. Tushar, S. Atanu Kumar and M. Belal Hossain Bhuian, "Vapor adsorption limitation of graphene nanoribbons in quasi conductance increment: A NEGF approach", *10th IEEE International Conference on Nano/Micro Engineered and Molecular Systems*, 2015.

[15] O. Leenaerts, B. Partoens and F. Peeters, "Adsorption of H_2O, NH_3, CO, NO_2, and NO on graphene: A first-principles study", *Physical Review B*, vol. 77, no. 12, 2008.

[16] Y. B. Zhang, Y. W. Tan, H. L. Stormer, and P. Kim, “Experimental observation of the quantum Hall effect and Berry‟s phase in graphene,” Nature, vol. 438, no. 7065, pp. 201–204, Nov. 2005.

[17] K. S. Novoselov, A. K. Geim, S. V. Morozov, D. Jiang, Y. Zhang, S. V. Dubonos, I. V. Grigorieva, and A. A. Firsov, “Electric field effect in atomically thin carbon films,” Science, vol. 306, no. 5696, pp. 666–669, Oct. 2004.

[18] A. K. Geim, “Graphene: Status and Prospects,” Science, vol. 324, no. 5934, pp. 1530–1534, Jun. 2009.

[19] M. Y. Han, B. Ozyilmaz, Y. B. Zhang, and P. Kim, “Energy band-gap engineering of graphene nanoribbons,” Phys. Rev. Lett., vol. 98, no. 20, p. 206805, May 2007.

[20]P. Dutta and P. Horn, "Low-frequency fluctuations in solids:1/f noise", *Reviews of Modern Physics*, vol. 53, no. 3, pp. 497-516, 1981.

[21]J. Berashevich and T. Chakraborty, "Tunable band gap and magnetic ordering by adsorption of molecules on graphene", *Physical Review B*, vol. 80, no. 3, 2009.